This is the peer-reviewed, final accepted version for American Mineralogist, published by the Mineralogical Society of America.
The published version is subject to change. Cite as Authors (Year) Title. American Mineralogist, in press.
DOI: https://doi.org/10.2138/am-2020-7486. http://www.minsocam.org/

Deciphering the enigmatic origin of Guyana's diamonds. (Revision 2)

Roy Bassoo[1*], Kenneth S. Befus[1], Peng Liang[1], Steven L. Forman[1], Glenn Sharman[2]

Key Words: diamond, Guyana, Guiana Shield, Roraima Supergroup.

Abstract

Diamonds have long been mined from alluvial terrace deposits within the rainforest of Guyana, South America. No primary kimberlite deposits have been discovered in Guyana, nor has there been previous studies on the mineralogy and origin of the diamonds. Paleoproterozoic terranes in Guyana are prospective to diamond occurrences because the most productive deposits are associated spatially with the eastern escarpment of the Paleoproterozoic Roraima Supergroup. Geographic proximity suggests that the diamonds are detrital grains eroding from the <1.98 Ga conglomerates, metamorphosed to zeolite and greenschist facies. The provenance and paragenesis of the alluvial diamonds are described using a suite of placer diamonds from different locations across the Guiana Shield. Guyanese diamonds are typically small, and those in our collection range from 0.3 to 2.7 mm in diameter; octahedral and dodecahedral, with lesser cubic and minor macle forms. The diamonds are further subdivided into those with abraded and non-abraded surfaces. Abraded diamonds show various colors in cathodoluminescence whereas most non-abraded diamonds appear blue. In all populations, diamonds are predominantly colorless, with lesser brown to yellow and very rare white. Diamonds are predominantly Type IaAB and preserve moderate nitrogen aggregation and total nitrogen concentrations ranging from trace to ~1971 ppm. The kinetics of nitrogen aggregation indicate mantle-derived residence temperatures of 1124 ± 100 ºC, assuming residence times of 1.3 Ga and 2.6 Ga for abraded and non-abraded diamonds respectively. The diamonds are largely sourced from the peridotitic to

[1] Baylor University, Department of Geosciences. One Bear Place, #97354, Waco, Texas, USA, 76798.
Roy_Bassoo1@Baylor.edu (*corresponding author)
[2] University of Arkansas, Department of Geosciences. 340 N. Campus Dr., Fayetteville, Arkansas, USA, 72701.

eclogitic lithospheric upper mantle based on both $\delta^{13}C$ values of -5.82 ± 2.45‰ (VPDB-LSVEC) and inclusion suites predominantly comprised of forsterite, enstatite, Cr-pyrope, chromite, rutile, clinopyroxene, coesite, and almandine garnet. Detrital, accessory minerals are non-kimberlitic. Detrital zircon geochronology indicates diamondiferous deposits are predominantly sourced from Paleoproterozoic rocks of 2079 ± 88 Ma.

Introduction

Diamonds have been mined for the past century from alluvial gravels along the rivers and creeks deep within Guyana's Amazon rainforest. The diamonds are found as placers in paleo-to-modern channels, terraces, and streambeds. Guyana's diamonds are found in headless placers, with the most productive gravels associated spatially with the eastern escarpment of the Roraima Supergroup, which suggests that the diamonds originate from this detrital source (Fig. 1). The humid tropical climate and ancient weathering profile of the Guiana Shield makes addressing diamond provenance a difficult task. Exploration has been driven by artisanal miners who prospect using detrital indicator minerals. No primary kimberlites are known in the region, and there is a lack of prior research on the nature and origin of diamonds in Guyana (e.g., Gibbs and Barron 1993, Shields and Letendre 1999, Persaud 2010).

Several hypotheses exist on the origin of Guyana's diamonds. Diamonds may be sourced from yet undiscovered primary kimberlites or igneous intrusions (Shields and Letendre 1999; Persaud 2010). The most likely location would be associated spatially with the highly magnesian ultramafic intrusives of the 1.7 ± 0.2 Ga, Badidku suite (Olszewski et al. 1977). These rocks intruded during a tectonically quiet period of the late Trans-Amazonian orogeny (Gibbs and Barron 1999) and might be associated with other ultramafic intrusions such as kimberlites. The only confirmed examples of primary diamond deposits in the Guiana Shield are in Guaniamo,

Venezuela, and Dachine, French Guiana (Fig. 1), where diamonds are found in Neoproterozoic kimberlite sills and metamorphosed Paleoproterozoic ultramafic and pyroclastic shoshonites or lamprophyres, respectively (Capdevila et al. 1999; Magee and Taylor 1999; Kaminsky et al. 2000; Channer et al. 2001; Kaminsky et al. 2004; Wyman et al. 2008; Smith et al. 2016). Kimberlites exist in Roraima, Brazil, but these are not diamondiferous (Svisero et al. 2017, Cabral et al. 2017). Known diamondiferous kimberlites from West Central Africa are an additional potential source for Guyana's alluvial deposits (Reid 1974 and Briceno 1984). These regions were immediately adjacent prior to the Jurassic rifting and opening of the Atlantic Ocean; separated by 200 to 400 km (Fig. 1). If diamonds were derived from Africa then they would be more prevalent in the northeastern Guiana Shield where diamonds are not found. Furthermore, West African diamonds have been traced to the host diamondiferous kimberlites which range in age from 92 – 846 Ma (Bardet and Vachette 1966; Andrews-Jones 1968; Hall 1972; Janse 1996; Fourie et al. 1998; Fourie et al. 2000; Kiviets 2003; Skinner et al. 2004). More locally, the Avanavero mafic dykes and sills (<1.79 Ga) have been suggested to be diamondiferous, but these dykes are tholeiitic norites and gabbros and thus unlikely to be diamond-bearing (Da Silva Rodrigues 1991; Reis et al. 2000; Heesterman et al. 2005). Finally, the diamonds may be derived as detrital grains weathering directly from diamondiferous conglomerates of the Paleoproterozoic Roraima Supergroup (e.g., Gibbs and Barron 1993; Meyer and McCallum 1993). This may be plausible because alluvial diamonds are sometimes found in gravels with abundant, rounded quartz, red jasper, and quartzite clasts; also observed in Roraima Supergroup conglomerates. Placer diamonds in Mutum, Brazil are mined from alluvial terraces shed possibly from conglomerates of the Tepequém Formation, which is equivalent to the Arai Formation pebbly sandstones and volcaniclastics of the Roraima Supergroup (Santos et

al. 2003; Reis et al. 2017). Similarly, in Suriname, diamonds are found in alluvium shed from metamorphosed Proterozoic conglomerates or ultramafic volcaniclastics of the Rosebel group, but their provenance remains unknown (van Kooten 1954; Schönberger and de Roeve 1974; Schönberger 1975; Bosma et al. 1983; Ramlal 2018; Naipal et al. 2019). The Roraima Supergroup and similar sedimentary sequences may have been a sink for diamonds erupted by unknown Paleoproterozoic kimberlites, and may be detrital evidence for some of Earth's earliest kimberlites.

Guyana's diamonds are a known commodity in the global diamond trade, referred to as "British diamonds," stemming from a colonial past. Economically valuable diamonds in Guyana are small, most commonly ranging from 0.1 to 0.4 carats although larger stones are found. Guyanese diamonds are predominantly colorless (G-J), yellow (K-M), and brown. Pink and green body colors are rare. Exploration activities conducted by Golden Star resources recovered alluvial diamonds and accessory minerals from Amatuk (Fig. 1) and are described as octahedral with moderate resorption textures. Green and brown spotting and skins are attributed to radiation damage from accessory zircon, monazite, uraninite, micas, and K-feldspar (Breeding et al. 2018), when residing in a placer environment. Surface abrasion and breakage post-dating resorption along crystal edges were interpreted to be derived from either a high energy fluvial environment or agitation during recovery (Shields and Letendre 1999).

We present the morphology, abrasion and dissolution textures, nitrogen concentration, carbon isotopic composition, and inclusion mineralogy of Guyana's alluvial diamonds to learn about their provenance, host magma characteristics, residence temperatures, and mantle source beneath the Guiana Shield. We characterize Guyana's diamonds and their accessory minerals, thereby facilitating meaningful comparisons with other diamond deposits in the Guiana Shield

and elsewhere. Diamonds were obtained from the Ekereku, Jawalla, Konawaruk, Kamarang, Kurupung, Maikwak, and Monkey Mountain alluvial deposits in Guyana (Fig. 1). Most diamonds crystallized from peridotitic lithosphere, although there is a lesser population of eclogitic diamonds. These diamonds can be divided into two basic groups; those with and without sedimentological abrasive textures. Importantly, non-abraded and abraded diamonds have statistically different cathodoluminescence, ultraviolet blue light luminescence, and Fourier Transform Infrared (FTIR) responses. Abraded diamonds are evidence for a detrital, polycyclic source weathering from the Roraima Supergroup. Non-abraded diamonds may be derived from the Roraima Supergroup, but have experienced less transport and recycling.

Regional Geology

Diamonds occur across the Guiana Shield and lesser portions of the Guaporé Shield within the Amazonian craton of South America (Fig. 1). The Guiana Shield is exposed for over 900,000 km^2 along the northern margin of the Amazonian Craton. Chemical weathering prevails throughout much of the Guiana Shield, resulting in thick sequences of saprolite capped by "tor" formations of large boulders of resistive and residual host rock, with the saprolite regolith stripped away by weathering (Kroonenberg and Gersie 2019). Although exposures are limited by accessibility and extreme tropical weathering, there is broad consensus that the Paleoproterozoic evolution of this craton was dominated by episodes of accretionary orogenic events around an Archean core complex during the Main Trans-Amazonian (2.26-2.08 Ga) to Late Trans-Amazonian (2.07-1.93 Ga) orogenies (Tassinari 1997; Vanderhaeghe et al. 1998; Reis et al. 2000; Delor et al. 2003; Cordani and Teixeira 2007; Fraga et al. 2009; Daoust et al. 2011; Kroonenberg et al. 2016).

The Guiana Shield is divided into four major Paleoproterozoic terranes (Daoust et al. 2011), one Mesoproterozoic terrane, and two isolated Archean terranes (Norcross 1997; Kroonenberg et al. 2016). Crustal development in the Guiana Shield created a series of greenstone belts, associated gneisses, and amphibolites of the Maroni-Itacaiunas Belt (Tassinari et al. 1997). The greenstone belts underwent several episodes of deformation, intrusion, and metamorphism between 2.26 Ga and 2.08 Ga, followed by cooling between 2.08 Ga and 1.93 Ga. These events are interpreted to reflect the expression of the Trans-Amazonian Orogeny in the Guiana Shield (Cordani and De Brito Neves 1982; Gibbs and Barron 1993; Norcross 1997; Daoust et al. 2011). Much of the region was then unconformably overlain by the Roraima Supergroup, which is a stratigraphic succession dominated by interbedded 1.98 - 1.78 Ga sandstones and conglomerates deposited from rocks eroding from earlier greenstone terranes (Priem et al. 1973; Santos et al. 2003). Finally, coeval mafic dykes of the Avanavero Suite intruded the entire sequence at ~1.79 Ga (Reis et al. 2000).

The region has been a stable craton, only modified by erosional processes, throughout much of the late Phanerozoic. The upper Proterozoic was marked by a period of prolonged uplift with no evidence of sedimentation (Gibbs and Barron 1993). Changing climate and repeated uplift cycles since the late Triassic have resulted in continuing surface evolution of the Guiana Shield. Rifting of South America from Africa beginning in the early Jurassic was associated with accelerated weathering and fluvial activity (McConnell 1968). The regional drainage patterns and depositional systems have evolved in response to millions of years of river capture, rejuvenation, degradation, and aggradation initiated by faulting and rifting since the opening of the Atlantic Ocean. Today the region preserves a complex network of high alluvial, terrace, alluvial flat, river bed, buried channel, and plateau deposits. Repeated cycles of erosion and

deposition have led to complex diamond placer deposits with detrital assemblages reflecting variable provenance and timing. The diamonds are found alongside accessory phases that include quartz, topaz, jasper, rutile, anatase, zircon, ilmenite, gold, corundum, and tourmaline, with minor garnet and chromite. Olivine and perovskite are notably absent. Diamond is the only residual mineral that certainly eroded from kimberlite rock. Despite the possibility for primary kimberlite sources and the complex geologic history of the Guiana Shield, placer deposits are the only diamond sources that have been discovered in Guyana.

Methods

We acquired a collection of diamonds from miners and a local diamond merchant (Kay's Diamond Enterprise Ltd.). We first cataloged each stone by measuring its dimensions and mass. The overall morphology of the diamonds was then assessed using a Zeiss Scope AX IO petrographic microscope. A focus was delineating crystal shape, dissolution textures, and abrasion. Some features were documented using high resolution scanning electron microscopy energy dispersive X-ray (SEM-EDS) spectroscopy at the Baylor University Center for Microscopy and Imaging.

The nitrogen content of 415 diamonds were measured, and the aggregation state calculated for the majority of samples using a Thermoscientific Nicolet iN10 FTIR spectrometer. Analyses were performed across 675-4000 cm^{-1} in cooled transmission mode using a 200 x 200 μm aperture size, 64 scans, and spectral resolution of 4 cm^{-1}. Nitrogen concentration was calculated from individual spectra by applying the Beer-Lambert law and absorption values of nitrogen bands at 1365, 1284, and 1175 cm^{-1}, using the least-squares fitting approach (e.g., Howell et al. 2012).

159 Effective thickness (x) was calculated by normalizing the absorption coefficient (μ) of
160 diamond lattice bands at 2443, 2158, and 2026 cm^{-1}, where $x = \mu_{2443}/5$; $x = \mu_{2158}/12$; $x = \mu_{2026}/12$
161 and the average effective thickness was then calculated (Kaminsky and Khachatryan 2012).
162 Stable carbon isotope analyses ($\delta^{13}C$, in $‰_{VPBD-LSVEC}$) were performed at the Baylor University
163 Stable Isotope Laboratory using a Costech Elemental Combustion System 4010 connected to a
164 Thermo-Electron Delta V Advantage continuous flow Isotope Ratio Mass Spectrometer (CF-
165 IRMS) through a Thermo Conflo IV interface. Fifty-seven crushed and powdered diamond
166 samples (<0.5mm) which range from 0.05 – 0.90 mg (mean - 0.26 ±0.15 mg) were loaded into
167 silver capsules, flash combusted at 1000ºC to convert the diamond to CO_2, which was carried to
168 the CF-IRMS by a constant helium gas flow.
169 Optical cathodoluminescence (CL) of 556 diamonds was observed using a Nikon-Japan
170 LV UEPI microscope equipped with a low vacuum Reliotron III that operated at 7.5-9 kV and
171 0.3-0.5 amps. The CL data was supplemented with ultraviolet blue light (UV) luminescence
172 (425-495 nm) observed in 558 diamonds using an Olympus BX51 petrographic microscope
173 equipped with an EXFO X-cite 120 fluorescence illumination system, with an exposure time of
174 approximately 10 s for most samples. Each crystal's color, or lack thereof, was documented for
175 both CL and UV observations.
176 Inclusions within 91 diamonds were identified using Raman spectra collected with a
177 Thermoscientific DXR Raman microscope equipped with a 532 nm laser operating at 8 mW, a
178 ~2-μm spot, and a high resolution 1800 lines mm^{-1} grating. Inclusion species were identified by
179 matching diagnostic peak positions and heights of unknown spectra with those in the RRUFF
180 spectral database (Lafuente et al. 2016).

Accessory minerals were extracted from heavy mineral separates that we collected from buried alluvial and colluvial deposits in the Kurupung region (UTM WGS 84 Zone 20N, 804678E, 675615N), approximately 4km from the base of the Roraima Supergroup escarpment. Rare diamonds were also recovered from these heavy mineral separates. Samples were sieved, separated by mass in a shaker table, and cleaned in a sonic bath. Hand-picked accessory minerals of garnet, chromite, and ilmenite were mounted in epoxy, polished at Baylor University and analyzed at the University of Texas at Austin, using a JEOL JXA-8200 Electron Microprobe (EPMA). Zircon crystals were also handpicked and analyzed for U-Pb crystallization ages using laser-ablation-inductively coupled plasma-mass spectrometry (LA-ICPMS) at the University of Arkansas Trace Element and Radiogenic Isotope Laboratory. For each sample, 150 detrital zircon grains were mounted on a glass slide using double-sided tape. Grain surfaces were ablated using an ESI 193 nm Excimer laser ablation system and a Thermo iCap quadropole ICP-MS. Data acquisition parameters include a 35 μm spot size, laser repetition rate of 10Hz, helium flow rate of 0.8 L min^{-1}, and a fluence of ~4.5 J cm^{-2}. Zircon from Plesovice (337.13 Ma; Slama et al., 2008) was used as a primary standard, with R33 (419 Ma; Black et al., 2004) as a secondary standard. The weighted mean average of R33 analyses was within 1% of the accepted age. Data were reduced in Iolite v. 3.71 (Paton et al., 2011), and individual analyses were manually trimmed to avoid zones of high discordance and ^{204}Pb bearing inclusions. Twenty-four analyses were excluded because they were not zircon or were contaminated by inclusions. An additional 17 zircon grains (5.6% of the total) were excluded on the basis of discordance ($^{207}Pb/^{206}Pb$ versus $^{206}Pb/^{238}U$) exceeded 10% or 5% reverse discordance. In total, 259 concordant zircon U-Pb analyses were retained (Fig. A1; Table A5).

Results

Morphology

Diamonds in our collection range in size from 0.3 to 2.7 mm in diameter; with a mean of 1.1 ± 0.2 mm. Masses range from 0.01 g to 0.95 g. Diamonds are predominantly colorless (93%) with lesser amounts of brown (4%) to yellow (3%) and very rare white (1%) variants (Fig. 2). Approximately half of the diamonds show no radiation spotting (55%). The remainder has green to green-blue skins or green spotting that covers up to ~100% of the surface area. A small population (5%) show combined overprinting of brown and green spotting (Table 1).

Diamonds across all regions are octahedral (30%) and dodecahedral (30%), with lesser combination (16%), flattened or elongate (15%), and cubic (3%) forms (Fig. 3) (Table 1). Those from Ekereku present more dodecahedrons (46%) than octahedrons (31%). Kamarang has the most flattened or elongated diamonds (26%), with the remainder being octahedral, dodecahedral, and various combinations. Twinned diamonds and aggregates are rare from any location. Fragments account for 9% of diamonds analyzed and resorbed fracture or fragmented diamond surfaces were not observed.

Fine stepwise, lamellar trigonal faces are common, whereas flat faces and sharp edges are uncommon (Fig. 3). Resorption textures, including terraces, tear drop hillocks, and dissolution pits are common in 95% of diamonds. Most octahedral diamonds have resorbed edges, and in the case of Ekereku, more diamonds are fully resorbed to dodecahedrons. Tear drop hillocks are the most common dissolution texture (Fig. 3f). The most common pit dissolution textures are flat bottom (37%) and point bottom (12%) trigons and tetragons (19%) (Table 2). Very fine (8%) to fine (3%) point bottom trigons are more abundant than coarse to very coarse point bottom trigons. Very fine (5%) to fine (14%) flat bottom trigons are slightly more abundant than coarse (12%) to very coarse (1%) flat bottom trigons. Point bottom hexagons, and trapezoids are

notably rare. Late stage etching features such as corrosion sculptures, shallow depressions, ruts, and glossy surfaces are observed in two-thirds of the diamonds. Less than 5% of diamonds show fine to medium microdisc textures, but when present occur in swarms.

Edge abrasion is found in 44% of abraded diamonds and is the most common sedimentologic-induced surface texture (Fig. 3i). Percussive marks along crystal edges, scratches, and crescentiform fissures are less common (Fig. 3j). Most diamonds have some degree of surface abrasion from minor scratches and edge abrasion and some have no apparent surface abrasion. This distinction in surface texture is the basis to subdivide Guyana's diamonds into abraded (85%) and non-abraded (15%) populations. Abraded diamonds may reflect an older population with extensive fluvial communition, whereas, the non-abraded diamond population may reveal a shorter distance and/or time of fluvial transport. Ekereku has the highest relative proportion of non-abraded diamonds followed by Kamarang and Kurupung, whereas Jawalla, Konawaruk, Monkey Mt., and Maikwak, have no abraded diamonds. Abraded diamonds average mass (9.3 ± 21.5 mg) is larger than that of non-abraded diamonds (5.5 ± 4.2 mg). Non-abraded diamonds are more dodecahedral in form (45% compared to 25%) (Table A1). Resorbed abraded diamonds present more flat-bottomed dissolution textures (85.3%) than point-bottom dissolution textures (18.7%). Non-abraded diamonds also present greater flat-bottomed dissolution textures (56.5%) than point-bottom dissolution textures (43.5%), but to a lesser degree (Table A1).

Cathodoluminescence and UV luminescence

Guyana's diamonds cathodoluminesce green (35%), blue (25%), and turquoise (18%) with lesser orange, red, and yellow (Table 3). Abraded and non-abraded diamonds demonstrate different responses to CL. Guyana's abraded diamonds dominantly show green CL (39%), turquoise (19%), and blue (19%), with minor orange, red, and yellow (~10%), with 11% non-

luminescent (Fig. 4a). In contrast, non-abraded diamonds cathodoluminesce blue (59%), minor green (13%), turquoise (10%), and orange (4%), with 13% showing no CL. No yellow or combination CL was observed. Statistical analyses (χ^2 tests) demonstrate with >99% certainty that the frequencies of CL response between abraded and non-abraded diamonds are independent (Table 4).

Ultraviolet luminescence also yields a clear distinction between abraded and non-abraded diamonds. Abraded diamonds UV luminesce green (84%) with very minor orange (1%), red (2%), and yellow (3%) variants, and 10% with no apparent luminescence. In contrast, non-abraded diamonds show a smaller population of green-luminescent grains (52%), and minor populations of red- (1%) and yellow-luminescent (1%) grains. A large proportion of non-abraded diamonds yielded no luminescence response (45%) (Fig. 4b). We note that similar CL and UV response distributions are observed for all diamonds regardless of geographic location.

Nitrogen and Carbon isotope composition

The nitrogen concentration of diamonds range between trace (< 5 ppm ~ Type IIa) and 1971 ppm, with a mean of 315 ± 24 ppm and rare outliers from 1175 to 1971 ppm. Diamonds are predominantly Type IaAB, accounting for 53%, with Type 1aA at 22%, and Type IaB at 9%. 17% of the diamonds are Type IIa and thus show no nitrogen aggregation (Fig. 5). No Type IIb diamonds are observed.

Marked differences in nitrogen concentration exist between abraded and non-abraded diamonds (Table 4). Non-abraded diamonds have higher average nitrogen concentrations compared to abraded diamonds with means of 621 ± 47 ppm and 271 ± 21 ppm, respectively (Fig. 5; Table 4). The nitrogen concentrations of non-abraded diamonds preserve a more uniform distribution with lower skewness and kurtosis coefficients of 0.26 and 1.91, whereas the abraded

diamonds display a pronounced positive skewness (1.82) and a higher kurtosis (6.62) (Table 4; Fig. A1). Multivariate density Finite Mixture Modeling of nitrogen concentrations was applied to determine if subpopulations could be readily identified within the greater abraded and non-abraded diamond populations, based on the Bayesian Information Criteria which demonstrates that a 21 component mixture is the most appropriate choice (Fig. A2) (e.g., Schwartz, 1978; Galbraith and Green 1990; Liang and Forman 2019; McLachlan et al. 2019). The Finite Mixture Modeling identified ten distinct subpopulations within the abraded diamonds and seven subpopulations within the non-abraded diamonds (Table 4). The abraded and non-abraded diamonds may share six subpopulations, with nitrogen concentrations of 604 ± 48, 390 ± 48, 180 ± 16, 47 ± 3, 23 ± 1, and 4 ± 0.3 ppm. The non-abraded population may have one additional group centered at 968 ± 79 ppm, whereas the abraded diamonds may have additional populations at 13 ± 1, 84 ± 8, 1234 ± 99, and 1911 ± 150 ppm. Nitrogen concentrations reported here are average and bulk compositions intended to characterize the diamond populations as a whole. Heterogeneity within each individual diamond is expected but not elaborated further.

Guyanese diamonds have an average $\delta^{13}C$ value of -5.82 ± 2.45‰ with a range from -16.11 to -2.88‰. These $\delta^{13}C$ values are slightly more depleted than diamonds from Arenápolis and Boa Vista, Brazil, and are significantly more enriched in ^{13}C than those of Guaniamo, Venezuela (-15 ± 2.78‰), and Dachine, French Guiana (-24.65 ± 4.12‰) (Fig. 6). Diamonds from West and Central Africa preserve a mode of -3.5‰, making them more enriched than Guyana's diamonds (Cartigny et al. 2014). Abraded diamonds have an average $\delta^{13}C$ value of -6.11 ± 2.71‰ and non-abraded diamonds have an average $\delta^{13}C$ value of -5.06 ± 1.36‰. For comparative spectroscopy, luminescence, $\delta^{13}C$, morphology, and inclusion paragenesis of Guyana's diamonds please see supplementary Tables A1-A4.

Inclusions

Diamond-hosted inclusions in order of decreasing abundance include forsteritic olivine, enstatitic orthopyroxene, rutile, chromite, garnet, clinopyroxene, and coesite (Table 5). Epigenetic inclusions consist of graphite, which are restricted to internal fractures within the diamond or along relaxed inclusion margins. Sulfide inclusions are rare. Most primary inclusions of olivine and orthopyroxene are cubo-octahedral, whereas clinopyroxene are prismatic to elongate cubo-octahedral. Forsteritic olivine is the most common inclusion, found in 6.3% of all diamonds examined. When found, olivine occurs as single inclusions or in clusters. Olivine inclusions are colorless and range in size from ~ 5 to 500 μm. Orthopyroxene is found in 2.3% of diamonds. It is colorless and inclusions are ~ 5 to 550 μm across. Garnet inclusions occur in 0.6% of diamonds. Garnets range in size from ~ 25 to 200 μm. Three garnets are purple and one is red-brown.

Accessory mineral geochemistry

Guyana's alluvial diamond deposits are frequently found with non-kimberlite water worn quartz, topaz, jasper, rutile, anatase, zircon, ilmenite, gold, corundum, and tourmaline, with minor garnet and chromite. Traditional kimberlite indicator minerals are uncommon but chromite, garnet, and ilmenite occur in our samples (Table A4). Two populations of mantle derived and crustal derived garnets are observed based on discrimination diagrams of Schulze et al. 2003 (Fig. 7). Crustal garnets are Mn-rich spessartines ($Alm_{27\pm19}Py_{2\pm5}Sp_{70\pm23}$). The mantle derived garnets ($Alm_{3\pm3}Py_{12\pm2}Sp_{84\pm3}$) are also low Cr and have moderately low TiO_2 (~ 0.19 wt%). SEM-EDS profiles of both garnet populations show no obvious compositional zoning or evidence of metamorphic overprint. Accessory ilmenite grains are MgO poor (0.17 ± 0.4 wt%) and TiO_2 rich ulvospinels (72.2 ± 7.6 wt%) ($Wu_{72\pm16}Ru_{28\pm16}$). We analyzed chromite in our

samples and compared them to previous analyses of accessory chromite conducted by Goldenstar resources from diamondiferous alluvial deposits in Amatuk (Shields and Letendre 1999). Most chromites have moderate to low TiO_2 (0.5 ± 0.8 wt%) and Al_2O_3 (14.2 ± 5.6 wt%) demonstrating magmatic arc (ARC) and mid ocean ridge basalt (MORB) affinities.

Detrital zircon geochronology

Two representative diamond-bearing heavy mineral separates from the Kurupung region were targeted for reconnaissance detrital zircon geochronology. The first was from colluvium in a raised terrace, approximately 3 m above the modern river (KU002). The second was collected from an alluvial gravel horizon within a buried fluvial channel. Most zircons are well rounded by abrasion. A minor proportion (~ 8%) of zircons occur as slightly abraded to non-abraded euhedral, doubly terminated prisms. Detrital zircon age distributions of both buried alluvium and terrace colluvium samples are dominated by zircon between 2.0 and 2.2 Ga in age; recording similar peak ages of 2.06 Ga and 2.04 Ga, respectively (Fig. A2). Only 5 grains of earliest Paleoproterozoic or Archean in age (i.e., > 2.3 Ga) were identified (~2% of the total), and these grains are generally late Archean (2.6-2.8 Ga) (Fig. 8). All zircon U-Pb analyses are older than the depositional age range of the 1.78 ± 0.03 Ga – 1.98 ± 0.08 Ga Roraima Supergroup (Santos et al. 2003).

Discussion

Guyana's alluvial diamond deposits represent an economic resource that also preserve valuable insights into the evolution of surface and subsurface processes of the Guiana Shield. Hypotheses regarding the mantle paragenesis and surface provenance of Guyana's diamonds exist, but each are based largely on speculation. Our morphology, composition, and inclusion

datasets provide empirical based reasoning to characterize the mantle conditions of diamond formation and identify the possible provenance of placer alluvial deposits.

The Guiana Shield has existed as a thick craton with lithospheric roots extending >130 km depth since at least 1.9 Ga (Gibbs and Barron 1993; Schulze et al. 2006). Such depths are enough to intersect the diamond stability field beneath the craton (Stachel and Harris 2009), depending on the thermal regime during that time. However, kimberlite deposits in Guyana have not been discovered, unlike elsewhere in the Guiana Shield (Kaminsky et al. 2000; Channer et al. 2001; Kaminsky et al. 2004; Svisero et al. 2017, Cabral et al. 2017). Instead, diamonds are recovered from Quaternary to modern alluvial deposits. Tectonic and sedimentologic processes may have mixed diamonds from different temporal and geographic sources into the same alluvial basins. Thus, Guyana's diamonds reflect complex surface and mantle processes across the Guiana Shield, since the Paleoproterozoic.

Paragenesis

Diamonds preserve both compositional and physical evidence of their parental mantle source. During crystal growth, diamonds may entrap particular suites of minerals as inclusions. Guyanese diamonds primarily contain inclusions of forsteritic olivine, enstatitic orthopyroxene, and chromite. This assemblage indicates most of the diamonds crystallized in, and were extracted from, the harzburgite peridotite dominated upper mantle. Less common diamonds preserve an eclogitic assemblage containing rutile, almandine garnet, clinopyroxene, and coesite inclusions. Cratonic lithospheric mantle assemblages are typically stable between 1 and 7 GPa and less than 1300°C (Mather et al. 2011). Both peridotite and eclogite assemblages spatially coexist beneath stable cratons, consistent with model geothermal gradients of 38-42 mWm^{-2} (Pollack and Chapman 1977; Stachel and Harris 2009).

364 The carbon isotopic composition of diamonds can be used to further resolve mantle
365 paragenesis. Guyana's diamonds yield an average $\delta^{13}C$ value of -5.82 ± 2.45‰ (Fig. 6), falling
366 within the range of -8 to -2‰ found in most P-type diamonds sampled from the peridotitic upper
367 mantle (Cartigny 2005). Few diamonds have values less than -10‰. These light $\delta^{13}C$ values are
368 E-type, having crystallized from eclogite and contain a possible organic carbon source derived
369 from metasedimentary rocks (Cartigny et al. 2014). Very light $\delta^{13}C$ values (< -16‰) might be
370 indicative of websteritic paragenesis (Deines and Harris 2004) but are rare in Guyana's
371 diamonds. Together, Guyana's diamond inclusion suites and carbon isotopic compositions
372 confirm that the diamonds are largely sourced from the lithospheric mantle and derived from
373 predominantly peridotite and eclogite rocks.
374 Accessory mineral compositions can also be used to infer the paragenesis of Guyana's
375 diamond deposits. Accessory garnet is spessartine ($Alm_{27\pm19}Py_{2\pm5}Sp_{70\pm23}$) in composition and
376 most are likely derived from granite and granodiorite rocks, which are common throughout the
377 Guiana Shield. A subpopulation of the spessartine preserves Mg/Ca ratios indicative of a mantle
378 derived affinity (Fig. 7; Mg#/Ca# ~ 3.80). These mantle spessartines ($Alm_{3\pm3}Py_{12\pm2}Sp_{84\pm3}$) have
379 low Cr and low TiO_2 concentrations and are likely derived from eclogitic source rocks (Schulze
380 et al. 2003). Although sourced from the mantle, these garnets are not likely of kimberlitic origin.
381 Instead, these low-Cr and low-TiO_2 spessartine were more likely derived from subducted oceanic
382 crust rich in Mn. In Guyana there are early Proterozoic manganiferous metasedimentary rocks
383 (Gibbs and Barron 1993); the largest of which are at Mathews Ridge which outcrops north of the
384 Roraima Supergroup (Westerman 1969). These could be remnants of subducted oceanic crust
385 from which the mantle affiliated garnets are derived. Accessory ulvospinels ($Wu_{72\pm16}Ru_{28\pm16}$) are
386 Mg-poor and are similarly derived from non-kimberlite mafic intrusions. Most chromites have

moderate to low TiO_2 and Al_2O_3 concentrations indicative of ARC and MORB tectonic environments which is typical of the Guiana shield; consisting of volcanic arc segments accreted over an Archean core (Tassinari 1997; Cordani & Teixeira 2007; Daoust et al. 2011; Reis et al. 2000; Fraga et al. 2009; Kroonenberg et al. 2016).

Paleo-thermal conditions of the mantle

The concentration and aggregation state of lattice bound nitrogen in diamond provides additional constraints on the crystallization temperature and mantle residence conditions of Guyanese diamonds. Nitrogen is the most abundant impurity in diamond, with concentrations sometimes reaching >0.3 wt% (Woods et al. 1990; Cartigny et al. 2001; Stachel and Harris 2009; Smart et al. 2011). Quantitative and FTIR derived nitrogen concentrations range from trace to 1971 ppm, with population means from different localities ranging between 120 and 620 ppm (Fig. 5a). Guyanese diamonds are predominantly Type I, including Type IaAB, Type IaA, and Type IaB. When compared to other South American diamonds (Kamarang, Kurupung, Konawaruk and Maikwak), nitrogen concentrations are within similar ranges to diamonds from Canastra and Arenápolis, Brazil (Table 6). The aggregation state of nitrogen within diamond is largely a function of residence temperature (Chrenko et al. 1977; Evans and Qi 1982). Kinetic modelling of the change in nitrogen aggregation state can be used to quantify the thermal evolution of the continental lithosphere and paleotectonic processes (Taylor et al. 1990). Individual total N ppm vs. $\%N_B$ (degree of nitrogen aggregation) ratios were used to calculate mean residence temperatures of 1124 ± 100ºC (Fig. 5) using the kinetics of the nitrogen A-B center aggregation reaction (e.g., Taylor et al. 1990; Taylor et al. 1996). Residence temperature distribution is slightly negatively skewed and slightly leptokurtic (Table 7). We considered a minimum age of eruption of 2.0 Ga and an assumed residence time of 1.3 Ga, if Guyana's

diamonds are derived from the Roraima Supergroup (maximum age of peridotitic diamonds ~ 3.3 Ga – maximum age of Roraima Supergroup ~ 2.0 Ga). We also considered the possibility that Guyana's diamonds might be derived from more recent kimberlites, of which the youngest of the Guiana Shield have an eruption age of ~ 0.7 Ga (Channer et al. 2001) and an assumed residence time of 2.6 Ga (maximum age of peridotitic diamonds 3.3 Ga – maximum age of Guaniamo kimberlites ~ 0.7 Ga). Assumptions regarding residence times ranging from the Paleoproterozoic of 1.3 Ga and Neoproterozoic of 2.6 Ga vary residence temperature by less than 3%. These formation temperatures indicate that both diamond populations can be derived from similar thermal conditions beneath the Guiana Shield, despite a wide range in possible emplacement ages. Projecting the average residence temperature along geothermal gradients of 38 - 42 mW/m^2 gives minimum crystallization depths between 165 and 185 km, which is evidence for crystallization in the lithospheric mantle (Stachel and Harris 2009).

Magma composition

Diamond habit, size, and form reflect crystal development during growth in the mantle, whereas dissolution and abrasion textures reveal resorption during ascent and transport, respectively. Guyana's diamonds are predominantly octahedral (Fig. 3a), indicating slow growth in near-equilibrium conditions found beneath a thick and stable subcratonic lithosphere in the diamond stability field (Harrison and Tolansky 1964; Seal 1965; Sunagawa 1984; Stachel and Harris 2009). Dodecahedrons (Fig. 3b) represent the second most common crystal habit for diamonds across Guyana; this form is particularly observed at Ekereku. Dodecahedrons may form in the mantle or during magmatic ascent via dissolution of octahedron apices and edges in response to disequilibria produced by high temperature oxidation in the presence of CO_2 and H_2O fluid phases (Fedortchouk et al. 2007). Diamond populations from other regions in Guyana

433 do not preserve a distribution so enriched in dodecahedral form, providing evidence for different
434 conditions of mantle departure or host magma volatile contents.

435 Additional aspects of the diamond-entraining magmatic fluid can be inferred from
436 dissolution features on crystal faces. Chemical oxidation caused by the interaction of fluid
437 volatile phases in a kimberlite or related rock, exploits surface defects on a diamond, causing it
438 to dissolve. Dissolution produces pits and hillocks, whose geometries are controlled by internal
439 dislocations, crystal defects, and intensive variables including pressure, temperature, and fO_2
440 (Fedortchouk 2015). Dissolution features (Fig. 3f) occur on 95% of the diamonds. Teardrop
441 hillocks are the most common resorption texture and indicate moderate resorption (Tappert and
442 Tappert 2011). Many different pit dissolution textures are recognized but are indistinguishable
443 amongst different geographic locations. Flat and point bottomed trigons, tetragons, and hexagon
444 pits are observed. Coarse flat bottom trigons are evidence for pre-eruptive mantle/melt
445 dissolution at temperatures ranging from 1250 to 1300°C (Fedortchouk 2015). Average diamond
446 residence temperatures of ~1120ºC and mantle/melt dissolution temperatures of 1250 to 1300°C
447 suggest diamonds encounter variable mantle thermal conditions during residence, such as higher
448 temperatures of kimberlitic melt during ascent. The greater abundance of flat bottom trigons
449 relative to point bottom trigons in abraded diamond populations indicates that the erupting host
450 magma was enriched in H_2O relative to CO_2 (Fedortchouk 2015). Experimental data confirm that
451 dissolution pit textures begin as point bottom features. In a fluid enriched in H_2O relative to
452 CO_2, dissolution of the diamond proceeds more rapidly in the lateral direction rather than the
453 vertical or {111} direction, creating coarse and flat-bottomed pits (Fedortchouk 2015). Late
454 stage etching microdisk textures (Fig. 3g) found on ~5% of the diamonds also provide evidence
455 for an H_2O-rich magma. These features form when the surface of the diamond is etched by a

456 H_2O fluid phase in the ascending host magma (Fedortchouk et al. 2007). Kimberlite magmas are
457 inferred to be often CO_2-rich and have a high CO_2/H_2O ratio (Sparks 2013). The dissolution
458 textures observed in Guyana's diamonds instead suggest that both abraded and non-abraded
459 diamond populations were hosted by a magma with more H_2O, and therefore a lower CO_2/H_2O
460 ratio. This characteristic is more commonly inferred for lamproitic melts (Bergman 1987;
461 Mitchell and Bergman 1991) although H_2O-rich kimberlite melts are possible (e.g., Ekati mine
462 kimberlites, see Fedortchouk et al. 2010). Because the non-abraded diamonds present a greater
463 proportion of point bottom dissolution textures than abraded diamonds, these diamonds may
464 have been entrained in a different host melt with a different ratio of H_2O/CO_2.

465 **Abraded versus non-abraded diamonds**

466 Diamond is strongly resistant in the natural environment to abrasion. It is brittle, which
467 permits only microcleavage abrasion in the faceting process, and it is extremely hard (Wilks and
468 Wilks 1972; Oganov et al. 2013). Accordingly, percussive marks, scratches, and edge abrasion
469 textures require repeated cycles of erosion, transport and deposition and/or a lengthy residence
470 time within surface environments. Using abrasion textures, we recognized two populations of
471 alluvial diamonds. Pristine, non-abraded diamonds account for 15% of all diamonds. Ekereku
472 has the highest relative proportion of non-abraded diamonds. Jawalla, Konawaruk, Maikwak and
473 Monkey Mt. have no abraded diamonds, but we acknowledge that the sample sizes from those
474 regions are small.

475 The non-abraded stones are found in the same deposits as the abraded diamonds.
476 Nitrogen concentrations indicate that non-abraded and abraded groups may have statistically
477 distinct subpopulations, six of which are common to both groups. These shared subpopulations
478 suggest that some diamonds are sourced from similar mantle residence and thermal conditions.

The distinct subpopulations identified in only the abraded or non-abraded groups may reflect isolated mantle and emplacement conditions. Statistically distinct spectroscopic responses between abraded and non-abraded populations also present evidence for different provenance and source (Table 4). Ultraviolet luminescence responses in abraded diamonds are overwhelmingly green and non-responsive, whereas non-abraded diamonds are split between non-responsive or green (Fig. 4). Luminescence is caused by the presence of impurities, such as nitrogen, and related defects which create vacancy centers in diamonds. Combined substitutional nitrogen and vacancy centers (H3 and H4 defects) within the diamond produced by irradiation followed by high temperature annealing are commonly ascribed to green luminescence (Shigley and Breeding 2013). This suggests that Guyana's abraded diamond population, which have a greater proportion of luminescent green stones were subjected to some form of metamorphic overprint. Abraded diamonds cathodoluminesce predominantly green, with moderate to minor blue and other colors. The majority of non-abraded diamonds cathodoluminesce blue. Worldwide, most diamonds from unmetamorphosed deposits cathodoluminesce blue with zero phonon line emissions at 415-440 nm and 480-490nm (Bulanova et al. 1995; Lindblom et al. 2005). This is attributed to the N3 defect where three nitrogen atoms surround a vacancy. With increasing grades of metamorphism and mild annealing at higher temperatures, nitrogen related defect centers become increasingly more complex and blue CL shifts to other colors, with emissions between 490-670 nm (Bruce et al. 2011; Kopylova et al. 2011). In diamond, vacancies and interstitials become more mobile at 500-800°C and ~300°C respectively (Clark et al. 1992; Collins et al. 2005; Collins and Kiflawi 2009). Enhanced diffusion and entrapment of vacancies and interstitials at higher temperatures at the site of various nitrogen forms to produce new optical centers is likely how blue CL shifts to other colors (Iakoubovskii and Adrianssens 1999;

Collins and Ly 2002). In the crust, these temperatures are typically inferred for zeolite to greenschist facies metamorphic environments. The abraded population likely experienced some metamorphic overprint. Comparatively, non-abraded diamonds may have been less metamorphosed. This can be also influenced by pre-existing nitrogen and vacancy related defects (N3, NV^o, and NVN) in Type Ia diamonds and manifest as photoluminescence emissions more commonly at 575 nm and less so at 430-450 nm but correlates rarely with cathodoluminescence (Bruce et al. 2011). Alternatively, irradiation damage during long placer residence would create charge vacancies and interstitials in the diamond lattice, which would also shift CL emittance from blue to other colors, but this damage is usually more common within the first 25 microns of the diamond surface (Vance et al. 1973; Breeding et al. 2018). Abraded diamonds are also larger in mass (9.3 ±2.2 mg) than non-abraded diamonds (5.5 ±4.2 mg), present fewer dodecahedral forms, and a greater ratio of flat-bottom to point-bottom dissolution textures (5:1 compared to 1:1). This is evidence that abraded and non-abraded diamond populations may have been entrained in different host melts. At present, both abraded and non-abraded populations are mixed into the same alluvial deposits, reflecting a complex interplay of mantle storage, eruptive history, and fluvial transport throughout the > 2.5 Ga evolution of the Guiana Shield.

Provenance

Abrasion, nitrogen concentration, CL, and UV observations indicate that alluvial deposits from each productive region across Guyana host both abraded, metamorphosed, nitrogen-poor diamonds as well as non-abraded, less metamorphosed, nitrogen-rich diamonds. Guyana's abraded diamonds are most likely derived from recycled paleo-placers with a metamorphic overprint. The probable source is the greenschist facies pebbly conglomerates or volcaniclastics of the 1.98 to 1.78 Ga Roraima Supergroup. Diamondiferous alluvial deposits occur in close

525 proximity to the margin of the Roraima Supergroup. In addition, diamond-bearing alluvial
526 deposits contain abundant quartzite and jasper clasts derived from the nearby Roraima
527 Supergroup. The Roraima Supergroup has been exposed at the surface since at least the early
528 Mesozoic (McConnell 1968). Increased weathering and erosion associated with rifting and
529 opening of the Atlantic since the Jurassic produced initial alluvial deposits derived from the
530 Roraima Supergroup, which have been continually exhumed and redeposited since that time by
531 repeated cycles of river capture, rejuvenation, degradation and aggradation (McConnell 1968,
532 Gibbs and Barron 1993). The majority of diamond populations in Guyana were likely abraded
533 within this complex polycyclic alluvial environment. Non-abraded diamonds were also likely
534 sourced from the Roraima Supergroup basal conglomerates and volcaniclastic horizons but were
535 trapped in sediment packages that experienced less energetic deposition, reworking and
536 experienced less metamorphic overprint and longer primary storage.

537 The Roraima Supergroup source is supported by comparison to alluvial diamond deposits
538 in Mutum, Brazil. Mutum diamonds are mined from alluvial terraces shed from conglomerates of
539 the Tepequém Formation in Brazil (Santos et al. 2003; Reis et al. 2017). The diamonds are
540 similar to Guyana's diamonds in size, skin color, $\delta^{13}C$, and nitrogen concentrations. These
541 diamonds, however, also present more flattened forms (60%), grey diamonds (40%), and fewer
542 proportions of diamonds with trigons (Araújo et al. 2011). This suggests that these diamonds
543 may be derived from a different magma source than Guyana's diamonds. The Arai Formation of
544 the Roraima Supergroup is the local age and lithologic equivalent of the Tepequém Formation.
545 Accordingly, conglomerates and volcaniclastics of the Arai Formation may be the detrital source
546 of Guyana's diamonds, representing a regional Paleoproterozoic high energy, siliciclastic

547 depositional basin that was a sink for diamonds emplaced by several episodes of kimberlite
548 volcanism within the Guiana Shield, during the middle Paleoproterozoic or older (>2.0 Ga).
549 Other hypotheses regarding the source of the diamonds have been put forward over the
550 past decades, including sources in West Africa, Boa Vista (Brazil), Dachine (French Guiana),
551 and Guaniamo (Venezuela). West Africa is home to kimberlite and alluvial diamond deposits.
552 Most diamonds from West Africa are alluvial in origin, but diamonds have also been mined from
553 kimberlites (Deines and Harris 1995; Skinner et al 2004). The alluvial diamonds are largely
554 weathered from Mesozoic kimberlite pipes and dykes. Colorless to brown body color and green
555 skins are common; similar to those in Guyana (Sutherland 1982; Janse 1996; Stachel et al. 2002).
556 Size and quality are inversely related to distance from the kimberlite source (Knopf 1970;
557 Norman et al. 1996; Grantham and Allen 1960; Janse 1996). The smallest carat sizes and best
558 quality gems are found in beach placers along the West African coastline. The oldest Mesozoic
559 sources may have produced microdiamonds that could have reached Guyana's eastern coast prior
560 to rifting associated with the Atlantic Ocean, but diamonds are not found on the coast. The more
561 recent Mesozoic kimberlites are too young and shed detrital diamonds into the juvenile Atlantic
562 Ocean instead. We conclude that Guyana's diamonds are unlikely to be related to sources in
563 West Africa.
564 The closest primary diamond-bearing igneous sources in the modern tectonic setting are
565 the Guaniamo kimberlite dykes in Venezuela and metamorphosed ultramafic and pyroclastic
566 shoshonites or lamprophyres in Dachine, French Guiana (Capdevila et al. 1999; Channer et al.
567 2001; Kaminsky et al. 2000; Kaminsky et al. 2004; Smith et al. 2016). Although some
568 similarities exist, including upper mantle temperatures, sizes, and colors between Guyana's and
569 Guaniamo's diamonds, we contend that those sources are unlikely to be genetically associated

570 with Guyanese diamonds based on geographic distance, distinct ^{13}C signatures, nitrogen
571 aggregation, predominantly eclogitic inclusions, and CL responses (Channer et al. 2001;
572 Kaminsky et al. 2000; Kaminsky et al. 2004). Furthermore, Dachine diamonds are smaller (< 1
573 mm), have a lower total nitrogen range from trace to 110 ppm, are strictly Ib to IaA, and have
574 mostly sulfide inclusions (Smith et al. 2016).

575 Detrital zircon geochronology provides additional compelling evidence supporting
576 provenance. Detrital zircon U-Pb ages from both colluvial and alluvial sediment demonstrate that
577 these diamondiferous deposits are likely derived from rocks of late Trans-Amazonian age, with
578 lesser contributions of Archean grains (Fig. 8). These deposits are inferred to be Pleistocene to
579 recent in age (McConnell 1968; Gibbs and Barron 1993). The similar ages between the diamond-
580 bearing colluvium and alluvium is consistent with the interpretation that both types of placer
581 diamond deposit are derived from similarly aged bedrock sources of the Barama-Mazaruni group
582 such as Surumu group volcaniclastics (Basei 1978; Schobbenhaus et al. 1994; Reis et al. 2017),
583 or alternatively, as inherited minerals from the once extensive Roraima Supergroup in a foreland
584 basin fill (Santos et al. 2003). The dominantly unimodal characteristic of these detrital zircon age
585 spectra is consistent with derivation from a relatively small geographic region, as a more multi-
586 modal age distribution would be expected if the diamond-bearing sediment was sourced from a
587 large fluvial catchment. Furthermore, the narrow range of ages suggesting a local geographic
588 origin, preponderance of coarse quartz and jasper lithic fragments, and presence of non-
589 kimberlitic or related rock type indicator minerals, lends evidence to the Roraima Supergroup
590 being the provenance area for the Guyana detrital zircons and diamonds.

591 **Implications**

In an environment prone to extreme tropical weathering, Guyana's diamonds are likely the only remaining mantle xenocrysts which can offer insight into volcanic and tectonic controls that existed during the early evolution of the Guiana Shield. Detrital zircon U-Pb ages suggest that the kimberlite or related rock sources that erupted Guyana's diamonds represent episodes of kimberlite volcanism during at least the middle Paleoproterozoic or during the Archean. Also, the surfaces of diamonds demonstrate they were emplaced by various mantle-derived melts enriched or balanced in H_2O relative to CO_2. Guyana's diamonds are likely xenocrysts from some of the Earth's oldest kimberlites or lamproites. These source rocks have long since eroded or are still undiscovered.

Guyana's diamonds are divided into two populations of recycled and abraded diamonds and primary and non-abraded diamonds. Both abraded and non-abraded diamonds, can be distinguished according to unique spectroscopic, luminescence and morphological characteristics. This classification can aid in characterizing the prospectivity of underexplored diamond fields, especially when other mantle xenocrysts are absent. The abraded diamonds are likely recycled detrital grains eroding from rocks of the Roraima Supergroup, which could therefore represent a regional placer diamond source terrane with a lateral extent of at least 450,000 km^2. The provenance of non-abraded diamonds still remains enigmatic. It may be that there are undiscovered primary kimberlites but it is more likely that these non-abraded diamonds may also be sourced from the Roraima Supergroup basal conglomerates and volcaniclastic horizons which have experienced less metamorphic overprint. Both diamond populations, inclusion suites, $\delta^{13}C$, and nitrogen concentrations suggest diamond formation at residence temperatures of approximately 1120°C in the peridotitic and eclogitic lithospheric mantle of the Guiana Shield.

Acknowledgements

We thank Marcus Harden of Alicanto Minerals and Gordon Nestor of the Guyana Geology and Mines Commission for their logistical support. Avalon Jagnandan of the Guyana Gold and Diamond Miners Association. Roy Melville and Nigel Blackman provided invaluable on field support, for which we are grateful. We also thank James Krakowsky (General Manager for Kays Diamond Enterprise Ltd), for technical advice and diamond samples, which were crucial to this study. A special thanks is given to Maya Kopylova of the University of British Columbia for her technical input. We thank Barry Schaulis at the University of Arkansas for assistance with LA-ICP-MS data collection.

References

Andrews-Jones, D.A. 1968. Petrogenesis and geochemistry of the rocks of the Kenema district, Sierra Leone (PhD thesis abs.). Leeds University, England.

Araújo, D.P., Santos, R.V., Souza, V., Chemale F. e Dantas, E. (2011) Diamantes Serra do Tepequém: resultados preliminares. 12th Simpósio da Amazônia, 2 a 5 de outubro de 2011 - Boa Vista - Roraima. Documento da Conferência.

Basei, M.A.S., and Teixeira, W. (1975) Geocronologia do Território de Roraima, in Anais, Conferência Geológica Intergüianas, 10th, Belém, Brazil: Belém, Brazil, Departamento Nacional de Pesquisa Mineral, 453–473.

Bassoo, R. and Murphy, B. (2018) The 9 Mile deposit of the Barama-Mazaruni Greenstone belt of the Guiana Shield: Geochemistry, geochronology and regional significance. Brazilian Journal of Geology, 48, 671-683.

636 Bardet, M.G., and Vachette, M. 1966. Determination d'ages de kimberlites de l'ouest African et
637 assai d'interpretation de dataions des diverses venus diamantiferes dans le monde. Bur.
638 Rech. Geol. Min. Rep. D866A59.
639 Bergman, S.C. (1987) Lamproites and other potassium-rich igneous rocks, a review of their
640 occurrence, mineralogy and geochemistry. Geological Society of London, Special
641 Publications, 30, 103 -190.
642 Bosma, W., Kroonenberg, S.B., van Lissa, R. V., Maas, K., and de Roever, E.W.F. (1983)
643 Igneous and metamorphic complexes of the Guiana Shield in Suriname. Geol. Mijnbouw,
644 62, 241-254.
645 Briceno, H.O. (1984) Genesis of Venezuelan mineral deposits II. Acta Scientifica Venezolana
646 36.
647 Breeding, C.M., Eaton-Magaña, S., and Shigley, J.E. 2018. Natural-color green diamonds: A
648 beautiful conundrum. Gems and Gemology. 54: 2-27.
649 Bruce, L. F., Kopylova, M.G., Longo, M., Ryder, J., and Dobrzhinetskaya, L.F. (2011)
650 Luminescence of diamonds from metamorphic rocks. American mineralogist, 96, 14-22.
651 Bulanova, G.P. (1995) The formation of diamond. Journal of Geochemical Exploration,
652 53, 1–23.
653 Cabral, N.I., Nannini, F., Silveira, F.V., Cunha, L.M., Bezerra, A.K., Souza, W.S. (2017) Mapa
654 das áreas kimberlíticas e diamantíferas dos estados de Roraima, Pará, Piauí, Rio Grande
655 do Norte, Santa Catarina e Rio Grande do Sul. Programa Geologia do Brasil (PGB), Ação
656 Avaliação dos Recursos Minerais do Brasil. Natal, CPRM, 2017, 1 mapa colorido, 215 x
657 90 cm. Escala 1:5,000,000.
658 Capdevila, R., Arndt, N., Letendre, J., Sauvage, J.F. (1999). Diamonds in volcaniclastic

659 komatiite from French Guiana. Nature, 399, 456–458.
660 Cartigny, P. (2005) Stables isotopes and the origin of diamond. Elements, 1, 79-84.
661 Cartigny, P., De Corte, K., Vladislav, S., Ader, M., De Parpe, P., Sobolev, N.K. and Javoy, M.
662 (2001) The origin and formation of metamorphic microdiamonds from the Kokchetav
663 massif, Kazakhstan: a nitrogen and carbon isotopic study. Chemical Geology, 176, 265-
664 281.
665 Cartigny, P., Palot, M., Thomassot, E., and Harris, J.W. (2014) Diamond formation: a stable
666 isotope perspective. Annual review of Earth and Planetary Sciences, 42, 699-732.
667 Channer, D.M.DER., Egorov, A. and Kaminsky, F. (2001) Geology and structure of the
668 Guaniamo diamondiferous kimberlite sheets, south-west Venezuela. Revista Brasileira de
669 Geociências, 31, 615-630.
670 Chrenko, R.M, Tuft, R.E., and Strong, H.M. (1977) Transformation of the state of nitrogen in
671 diamond. Nature, 20, 141-144.
672 Clark, C.D., Collins, A.T., and Woods, G.S. (1992) Absorption and luminescence spectroscopy.
673 In J.E. Field, Ed., The Properties of Natural and Synthetic Diamond, 35–69. Academic,
674 New York.
675 Collins, A., Connor, A., Ly, C-H., and Shareef, A. (2005) High-temperature annealing of optical
676 centers in type-I diamond. Journal of Applied Physics, 97, 083517.
677 Collins, A. and Kiflawi, I. (2009) The annealing of radiation damage in Type Ia diamond.
678 Journal of Physics: Condensed Matter, 21, 364209.
679 Collins, A. and Ly, C-H. (2002) Misidentification of nitrogen-vacancy absorption in diamond.
680 Journal of Physics: Condensed Matter, 14, L467–L471.

681 Cordani U.G. and Brito Neves B.B. (1982) The geologic evolution of South America during the
682 Archaean and early Proterozoic. Revista Brasileira de Geociências, 12,78-88.
683 Cordani U.G., Teixeira W. (2007) Proterozoic accretionary belts in the Amazonian Craton.
684 Geological Society of America Memoirs, 200, 297-320.
685 Da Silva Rodrigues, A.F. (1991) Depositos diamantiferos de Roraima, in Schobbenhaus, C.,
686 Queiroz, E.T., and Coelho, C.E.S., eds., Principais depositos minerais do Brasil. Rochas e
687 minerais industriais. Gemas e rochas ornamentais: Brasilia, Departmento Nacional de
688 Producao Mineral (DNPM)/Companhia de Pesquisa de Recursos Minerais (CPRM), 177-
689 198.
690 Daoust C., Voicu G., Brisson H. and Gauthier M. (2011) Geological Setting of the
691 Paleoproterozoic Rosebel gold district, Guiana Shield, Suriname. Journal of South
692 American Earth Sciences, 32, 222-245.
693 Deines, P., and Harris, J.W. (2004) New insights into the occurrence of ^{13}C-depleted carbon in
694 the mantle from two closely associated kimberlites: Letlhakane and Orapa, Botswana.
695 Lithos, 77, 125-142.
696 Deines, P., and Harris, J.W. (1995) Sulfide inclusion chemistry and carbon isotopes of African
697 diamonds. Geochemica Cosmochemica Atca, 59, 3173-3188.
698 Delor C., Lahondère D., Egal E., Lafon J.M., Cocherie A., Guerrot C., Rossi P., Truffert C.,
699 Théveniaut H., Phillips D. and de Avelar V.G. (2003) Trans-Amazonian crustal growth
700 and reworking as revealed by the 1:500,000 scale geological map of French Guyana (2nd
701 edition). Geology of France and surrounding areas. Special Guyana Shield, BRGM –
702 SGF, 2-3-4:5–57.

703 Evans, T. and Qi, Z. (1982) The kinetics of the aggregation of nitrogen atoms in diamond.
704 Proceedings of the Royal Society A, 381, 169-178.
705 Fedortchouk, Y., Canil, D., and Semenets, E. (2007) Mechanisms of diamond oxidation and their
706 bearing on the fluid composition in kimberlite magmas. American mineralogist, 92,
707 1200-1212.
708 Fedortchouk. Y (2015) Diamond resorption features as a new method for examining conditions
709 of kimberlite emplacement. Contributions to mineralogy and petrology. 170.
710 Fedortchouk, Y., Matveev, S., Carlson, J.A. (2010) H_2O and CO_2 in kimberlitic fluid as recorded
711 by diamonds and olivines in several Ekati Diamond Mine kimberlites, Northwest
712 Territories, Canada. Earth and Planetary Science Letters, 289, 549-559.
713 Fourie, L., Phillips, D., Kieviets, G., 1998. Ages of Koidu kimberlites, Sierra Leone,
714 Unpublished De Beers data.
715 Fourie, L., Barton, E., Kieviets, G., 2000. Ages of Guinea kimberlites, Sierra Leone,
716 Unpublished De Beers data.
717 Fraga, L.M.B., Macambira, M.J.B., Dall'Agnol and R., Costa, J.B.S. (2009) 1.94–1.93 Ga
718 charnockitic magmatism from the central part of the Guyana Shield, Roraima, Brazil:
719 single-zircon evaporation data and tectonic implications. Journal of South American
720 Earth Sciences, 27, 247-257.
721 Galbraith, R., and Green, P. (1990) Estimating the component ages in a finite mixture.
722 International Journal of Radiation Applications and Instrumentation. Part D. Nuclear
723 Tracks and Radiation Measurements, 17, 197-206.
724 Gibbs A.K. and Barron C.N. (1993) The Geologv of the Guiana Shield. Oxford University Press,
725 New York.

Grantham, D.R., and Allen, J.B. (1960) Kimberlite in Sierra Leone. Overseas Geology and Mineral Resources, 8(1), 5-25.

Hall, P.K. 1972. The diamond fields of Sierra Leone. Geological Survey of Sierra Leone Bulliten. 5(1): 133

Harrison, E.R., and Tolansky, S. (1964) Growth history of a natural octahedral diamond. Proceedings of the Royal Society of London. Series A, mathematical and physical sciences, 279, 490-496.

Heesterman, L., Kemp A.W., Arjune B.K., and Cole, E. (2005) Pashanamu project geology, structure and geochemistry. Guyana Geology and Mines Commission.

Howell, D., O'Neill, C. J., Grant, K. J., Griffin, W. L., Pearson, N. J., and O'Reilly, S. Y. (2012) μ-FTIR mapping: distribution of impurities in different types of diamond growth. Diamond and Related Materials, 29, 29-36.

Iakoubovskii, K. and Adriaenssens, G.J. (1999) Photoluminescence in CVD diamond films. Physica Status Solidi Applied Research, 172, 123–129.

Janse, A.J.A. (1996) A history of diamond sources in Africa: Part II. Gems and Gemology.

Kaminsky, F.V., and Khachatryan, G. (2012) Nitrogen in diamond. KM Diamond Exploration, Ltd. West Vancouver, Canada. Indian Institute of Technology, Mumbai.

Kaminsky F.V., Zakharchenko O.D., Khachatryan G.K., and Shiryaev A.A. (2001) Diamonds from the Coromandel area, Minas Gerais, Brazil. Revista Brasileira de Geociências, 31, 583-596.

Kaminsky, F.V., Sablukov, S.M., Sablukova, L.I. and Channer, D.M.DER. (2004) Neoproterozoic “anomalous” kimberlites of Guaniamo, Venezuela: mica kimberlites of “isotopic transitional” type. Lithos, 76, 565-590.

Kaminsky, F.V., Zakharchenko O.D., Khachatryan G.K., Griffin W.L., and Channer D.M.DeR. (2006). Diamond from the Los Coquitos area, Bolivar State Venezuela. The Canadian Mineralogist, 44, 323-340.

Kaminsky, F.V., Zakharchenko, O.D., Griffin, W.L., Channer, D.M.DER. and Khacchatryan-Blinova, G.K. (2000). Diamond from the Guaniamo area, Venezuela. Can. Mineral, 38, 1347-1370.

Kiviets, G.B. 2003. 40Ar/39Ar laser probe analysis of phlogopite from two samples from the Weasua area, Western Liberia. Unpublished De Beers data.

Knopf, D. (1970) Les kimberlites et les roches apparentés de Côte d'Ivoire (Kimberlite and related rocks of Ivory Coast). Sodemi, Abidjan. pp 202.

Kopylova, M., Afanasiev, V.P., Bruce, L.F., Thurston, P.C., and Ryder, J. (2011) Metaconglomerate preserves evidence for kimberlite, diamondiferous root and medium grade terrane of a pre-2.7 Ga Souther Superior protocraton. Earth and Planetary science letters, 312, 231-225.

van Kooten, C. (1954) Eerste onderzoek op diamant: Rosebel-Sabanpassie. Mededeling Geologisch Mijnbouwkundige Dienst, Suriname 11, 63-64 pp.

Kroonenberg S.B., De Roever E.W.F., Fraga L.M., Reis N.J., Faraco M.T., Cordani U.G., Lafon J.M. and Wong, Th. E. (2016) Paleoproterozoic evolution of the Guiana Shield in Suriname - a revised model . Netherlands Journal of Geosciences, 95, 491-522.

Kroonenberg, S.B., and Gersie, K. (2019) Quaternary climate change and its importance for gold exploration in the Guiana Shield. Conference paper. 11th Inter Guiana Geological Conference, Paramaribo, Suriname, 19-20 February, 2019.

771 Lafuente, B., Downs, R. T., Yang, H., and Stone, N. (2016) The power of databases: the RRUFF
772 project. In Highlights in mineralogical crystallography (pp. 1-29). Walter de Gruyter
773 GmbH.
774 Liang, P., and Forman, S. (2019) LDAC: Luminescence dose and age calculator (v 1.0)
775 [computer software]. Luminescence dating research lab. Baylor University.
776 Lindblom, J., Holsa, J., Papunen, H., and Hakkanen, H. (2005) Luminescence study of defects in
777 synthetic as-grown and HPHT diamonds compared to natural diamonds. American
778 Mineralogist, 90, 428–440.
779 Mather, K.A., Pearson, D.G., McKenzie, D., Kjarsgaard, B.A., and Priestly, K. (2011)
780 Constraints on the depth and thermal history of the cratonic lithosphere from peridotite
781 xenoliths, xenocrysts and seismology. Lithos, 125, 729-742.
782 Magee, C.W. and Taylor, W.R. 1999. Diamond and chromite geochemical constraints on the
783 nature of the Dachine complex, French Guiana, Annual Report. Australian National
784 University, Canberra, Australia: 85.
785 McConnell, R.B. (1968) Planation surfaces in Guyana. The Geographical Journal, 134, 506-520.
786 McLachlan, G. J., Lee, S. X., and Rathnayake, S. I. (2019) Finite Mixture Models: Annual
787 Review of Statistics and Its Application, 6(1), 355-378.
788 Meyer, H.O.A, and McCallum, M.E. (1993) Diamonds and their sources in the Venezuelan
789 portion of the Guyana Shield. Economic Geology, 88, 989-998.
790 Mitchell, R.H. and Bergman, S.C. (1991) Petrology of lamproites. Plenum Press. New York and
791 London.

792 Nadeau, S., and Heesterman, L. (2010) Guyana Geology and Mines Commission, Geological
793 Map of Guyana - scale 1: 1 million. Guyana Geology and Mines Commission,
794 Georgetown, Guyana.
795 Naipal, R., Kroonenberg, S., and Mason, P. (2019) Ultramafic rocks of the Paleoproterozoic
796 greenstone belt in the Guiana Shield of Suriname, and their mineral potential. SAXI- XI
797 Inter Guiana Geological Conference 2019: Paramaribo, Suriname.
798 Norcross C.E. (1997) U-Pb Geochronology of the Omai Intrusion Hosted Au- Quartz Vein
799 Deposit and Host Rocks, Guiana Shield, South America. A Thesis submitted in
800 conformity with the requirements for the degree of Master of Science, Graduate
801 Department of Geology, University of Toronto. University of Toronto.
802 Norman, D.I., Ward, J., McKittrick, S. (1996) Hosts and sources of Ghana diamonds. Paper
803 given at the SME/AIME annual meeting, Phoenix, Arizona, USA.
804 Oganov, A., Hemley, R.J., Hazen, R.M. and Jones, A.P. (2013) Structure, Bonding, and
805 Mineralogy of Carbon at Extreme Conditions. Reviews in Mineralogy and Geochemistry,
806 75. 47-77.
807 Olszewski, W.J., Jr., and Gaudette, H., and Mendonza, V. 1977. Rb-Sr geochronology of the
808 basement rocks, Amazonas Territory, Venezuela: a progress report. Proc. V Congreso
809 Geologico Venezolano, 2: 519-525.
810 Paton, C., Hellstrom, J., Paul, B., Woodhead, J., & Hergt, J. (2011). Iolite: Freeware for the
811 visualisation and processing of mass spectrometric data. Journal of Analytical Atomic
812 Spectrometry, 26(12), 2508.
813 Persaud, K. (2010) The diamond industry and exploration for diamonds in Guyana, Guyana
814 Geology and Miners Commission.

Pollack, H.N. and Chapman, D.S. (1977) On the regional variation of heat flow, geotherms and lithospheric thickness. Tectonophysics, 38, 179-196.

Priem H.N.A., Boelrijk N.A.I.M, Hebed E.H., Verdurmen E.A., Verschure R.H. (1973) Age of the Precambrian Roraima Formation in Northeastern South America: Evidence from Isotopic Dating of Roraima Pyroclastic Volcanic Rocks in Suriname. 84, 1677-1684.

Ramlal, S. (2018) An investigation of the Brincks intrusion and its relationship to the surrounding gold deposits, Brokopondo, Suriname, South America. MSc thesis. Anton de Kom University of Suriname, 146-147.

Reid, A.R. (1974) Proposed origin for Guianian diamonds. Geology, 2, 67-68.

Reis N.J., de Faria M.S.G., Fraga L.M. and Haddad R.C. (2000) Orosirian calc-alkaline volcanism and the Orocaima event in the northern Amazonian Craton, eastern Roraima State. Revista Brasileira de Geociências, 30, 380-383.

Reis, N.J., Nadeau, S., Fraga, L.M., Betiollo, L.M., Faraco, M.T.L., Reece, J. Lachhman, D. and Ault, R. (2017) Stratigraphy of the Roraima Supergroup along the Brazil-Guyana border in the Guiana Shield, Northern Amazonian Craton – results of the Brazil-Guyana Geology and Geodiversity mapping project. Brazillian Journal of Geology, 47, 43-57.

Santos, J.O.S., Potter, P.E., Reis, N.J., Hartman, L.A., Fletcher, I.R., McNaughton, N.J. (2003) Age, source and regional stratigraphy of the Roraima Supergroup and Roraima-like outliers in northern South America based on U–Pb geochronology. Geological Society of America Bulletin, 115, 331–348.

Schobbenhaus, C., Hoppe, A., Lork, A., and Baumann, A. (1994) Idade U/Pb do magmatismo Uatumã no norte do cráton Amazônico, Escudo das Guianas (Brasil): Primeiros

resultados, in Anais, Congresso Brasileiro de Geologia, 37th, Camboriú, Brazil: Porto Alegre, Brazil, Sociedade Brasileira de Geologia, 2, 395–397.

Schönberger, J.M.H., (1975) Diamond exploration between the Suriname and Saramacca Rivers (NE Suriname) . Mededeling Geologisch Mijnbouwkundige Dienst 23, 228-238.

Schönberger, H, and de Roever, E.W.F. (1974) Possible origin of diamonds in the Guiana Shield: Comment. Geology, 2, 475-475.

Schulze, D.J. (2003) A classification scheme for mantle-derived garnets in kimberlite: a tool for investigating the mantle and exploring for diamonds. Lithos, 71, 195-213.

Schulze, D. J., Canil, D. M., Channer, D. M. DeR., Kaminsky, F.V. (2006) Layered mantle structure beneath the western Guyana Shield, Venezuela: Evidence from diamonds and xenocrysts in Guaniamo kimberlites. Geochimica et cosmochimica Acta, 70, 192-205.

Schwartz, G. (1978). Estimating the dimensions of a model. Annals of Statistics 6, 461-464.

Seal, M. (1965) Structure in diamonds as revealed by etching. American Mineralogist, 50, 105-123.

Sharman, G. R., Sharman, J. P., & Sylvester, Z. (2018). DetritalPy: A Python-based toolset for visualizing and analysing detrital geo-thermochronologic data. The Depositional Record, 4(2), 202-215.

Shields, H.N and Letendre, J. (1999) Final Exploration Report on Amatuk Prospecting License for the period January 2, 1996 to February 9, 1998. Golden Star Resources Ltd.

Shigley, J.E., and Breeding, M. (2013) Optical defects in diamond: a quick reference chart. Gems and Gemology, 49.

Skinner, E.M.W., Apter, D.B., Morelli, C., and Smithson, N.K. 2004. Kimberlites of the Man Craton, West Africa. Lithos. 76: 233-259.

Slama, J., Košler, J., Condon, D.J., Crowley, J.L., Gerdes, A.E., Hanchar, J.M., Horstwood, M.S., Morris, G.A., Nasdala, L., Norberg, N.S., Schaltegger, U., Schoene, B., Tubrett, M., & Whitehouse, M.J. (2008). Plešovice zircon: a new natural reference material for U-Pb and Hf isotopic microanalysis.

Smart, K., Chacko, T., Stachel, T., Muehlenbachs, K., Stern, R., and Heaman, L. (2011) Diamond growth from oxidized carbon sources beneath the Northern Slave Craton, Canada: a δ^{13}C-N study of eclogite-hosted diamonds from the Jericho kimberlite. Geochimica et Cosmochimica Atc, 75, 6027-6047.

Smith, B.M., Walter J.W., Galina P.B., Mikhail S., Burnham A.D., Gobbo L., and Kohn S.C. (2016) Diamonds from Dachine, French Guiana: A unique record of early Proterozoic subduction. Lithos, 265, 82-95.

Stachel, T and Harris, J.W. (2009) Formation of diamond in the Earth's mantle. Journal of Physics: Condensed Matter, 21, 364206 (10pp)

Stachel, T., Harris, J.W., Aulbach, S., and Deines, P. (2002) Kankan diamonds (Guinea) III: δ^{13}C and N characteristics of deep diamonds. Contributions to mineralogy and petrology, 142, 465 – 475.

Sunagawa, I. (1984) Morphology of natural and synthetic diamond crystals. In: I. Sunagawa (editor) Materials science of the Earth's interior. Terra Scientific, Tokyo, 303-330.

Sutherland, D.G. (1982) The transport and sorting of diamonds by fluvial and marine processes. Econ. Geol., 77, 1613-1620.

Svisero, D.P., Shigley, J.E., and Weldon, R. (2017) Brazilian diamonds: A historical and recent perspective. Gems and Gemology. 53(1).

882 Tappert, R. and Tappert, M. (2011) Diamonds in nature: A guide to rough diamonds. Springer
883 Heidelberg Dordrecht London New York.
884 Tappert, R., Stachel, T., Harris, J.W., Muehlenbachs, K. and Brey, G.P. (2006) Placer diamonds
885 from Brazil: Indicators of the composition of the Earth's mantle and the distance to their
886 kimberlitic sources. Economic Geology, 101, 453-470.
887 Tassinari C.C.G. (1997) The Amazonian Craton. In: De Wit M.J. and Ashwal M.J. (Editors),
888 Greenstone Belts. Clarendon Press, Oxford 558-566.
889 Taylor, W.R., Canil, D., Milledge, H.J. (1996) Kinetics of Ib to IaA nitrogen aggregation in
890 diamond. Geochimica et Cosmochimica Acta, 60, 4725-4733.
891 Taylor, W.R., Jaques, A.L. and Ridd, M. (1990) Nitrogen-defect aggregation characteristics of
892 some Australasian diamonds: Time-temperature constrains on the source regions of pipe
893 and alluvial diamonds. American Mineralogist, 75, 1290-1310.
894 Vance, E.R., Harris, J.W., and Milledge, H.J. (1973) Possible origins of α damage in diamonds
895 from kimberlite and alluvial sources. Mineralogical magazine. 39, 349-360.
896 Vanderhaeghe O., Ledru P., Thiéblemont D., Egal E., Cocherie A., Tegyey M. and Milési J.P.
897 (1998) Contrasting mechanism of crustal growth Geodynamic evolution of the
898 Paleoproterozoic granite greenstone belts of French Guiana. Precambrian Research,
899 92, 165-193.
900 Westerman, A.R. 1969. A structural analysis of Mathews' ridge Mn mine – with an appendix on
901 supergene enrichment. Conference paper: Guiana geological conference. 8.
902 Wilks, E.M. and Wilks, J. 1972. The resistance of diamond to abrasion. Journal of physics D:
903 Applied physics. 5: 1902-1919.

Woods, G.S., Van Wyk, J.A. and Collins, A.T. (1990) The nitrogen content of type Ib synthetic diamond. Philosophical Magazine B, 62, 589-595.

Wyman, D.A., O'Neill, C., Ayer, J.A. 2008. Evidence for modern-style subduction to 3.1 Ga; a plateau-adakite-gold (diamond) association. In; Condie, K.C., Pease, V. (Eds.), When did plate tectonics begin on planet earth: 129-148.

Xie, X., Mann, P., & Escalona, A. (2010). Regional provenance study of Eocene clastic sedimentary rocks within the South America–Caribbean plate boundary zone using detrital zircon geochronology. Earth and Planetary Science Letters, 291(1-4), 159-171.

Figure captions

Figure 1. Geological Map of the Guiana Shield and inferred adjacent West African craton during the Jurassic, showing primary and placer diamond deposits. (AM – Amatuk, AR – Arenápolis, BA – Baoule, BV – Boa Vista, CA – Canastra, CO – Los Coquitos, CR – Coromandel, DC – Dachine, EK – Ekereku, GU – Guaniamo, JW – Jawalla, KM – Kamarang, KU – Kurupung, KW – Konawaruk, MG – Mano Gadua, MK – Maikwak, MM – Monkey Mt., NA – Nassau, RO – Rosebel, SE – Seguela, TE – Tepequém, TO – Tongo, TY – Tortiya) (Modified from Santos et al. 2003, Nadeau and Heesterman 2010, Daoust et al. 2011, Kroonenberg et al. 2016, and Bassoo and Murphy 2018).

Figure 2. Body and skin color. a) colorless, b) white, c) yellow, d) brown, e) brown skins f) green skins

Figure 3. Morphological features. a) octahedral, b) dodecahedral, c) flattened/macle, d) trigons, e) hexagons, f) hillocks, g) microdiscs, h) fully abraded, i) edge abrasion, j) percussive marks

927 Figure 4. Cathodoluminescence and UV luminescence optical responses.

928 Figure 5. Nitrogen aggregation of Guyana's diamonds. a) Total N (ppm) vs N_B (%) plot of
929 abraded and non-abraded diamonds (Total N ± 24 ppm, $\%N_B$ ± 1.7%), b) nitrogen
930 aggregation type classification, c) representative FTIR spectrum showing carbon and
931 nitrogen in diamond regions.

932 Figure 6. $\delta^{13}C$ values (in $\%_{VPDB\text{-}LSVEC}$) of Guyana's diamonds compared to other South
933 American diamonds. ([1]Tappert et al. 2006; [2]Kaminsky et al 2000; [3]Smith et al. 2016)

934 Figure 7. Ca# vs Mg# plot of mantle and crustal derived accessory garnets (Schulze et al. 2003).

935 Figure 8. Comparative detrital zircon U-Pb age distributions from alluvial and colluvial samples
936 at Kurupung.

937 **Supplementary figure captions**

938 Figure A1. Kernel density plot of N (ppm) between a) abraded and b) non-abraded diamonds,
939 and c) Bayesian Information Criteria vs component plot showing a 21 component mixture
940 as the most appropriate number of nitrogen populations of the FMM.

941 Figure A2. Detrital zircon U-Pb age distributions plotted as a) cumulative and b) relative
942 probability density plots (Sharman et al. 2018). Vertical grey bar indicates the
943 depositional age range of the Roraima Supergroup. Peak ages are labeled.

944 **Table captions**

945 Table 1. Summary morphology.

946 Table 2. Pit dissolution textures of Guyana's diamonds.

947 Table 3. Optical spectroscopy.

948 Table 4. Spectroscopic comparisons between abraded and non-abraded diamonds.

949 Table 5. Guyana diamond inclusion types.

950 Table 6. Nitrogen concentrations of Guiana Shield diamonds.

951 Table 7. Formation temperatures of Guiana Shield diamonds.

952 **Supplementary table captions**

953 Table A1. Abraded vs non-abraded diamond comparisons.

954 Table A2. Comparative FTIR and δ13C of Guyana's diamonds.

955 Table A3. Comparative FTIR derived N concentrations, residence temperatures, CL, and UV
956 responses for Guyana's diamonds.

957 Table A4. Accessory mineral compositions (wt%).

958 Table A5. U-Th-Pb ages of detrital zircons from diamondiferous alluvium and colluvium
959 analyzed at the University of Arkansas.

960 **End**

This is the peer-reviewed, final accepted version for American Mineralogist, published by the Mineralogical Society of America.
The published version is subject to change. Cite as Authors (Year) Title. American Mineralogist, in press.
DOI: https://doi.org/10.2138/am-2020-7486. http://www.minsocam.org/

Figure 1

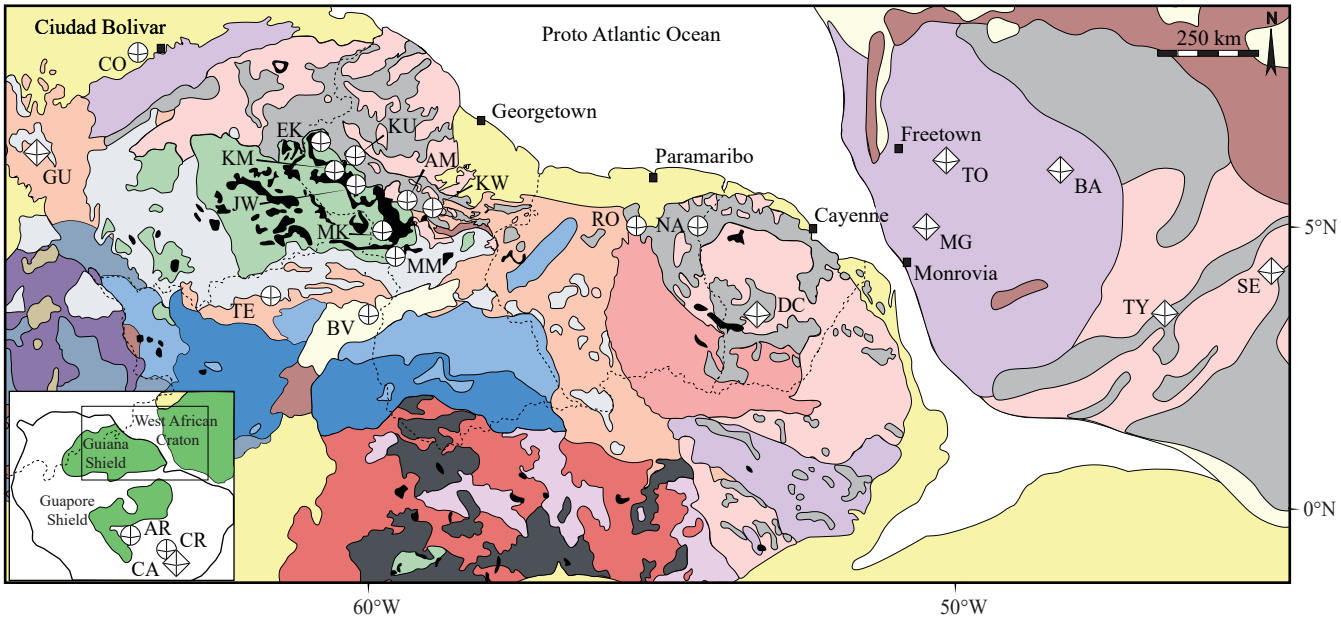

Figure 1 - Legend

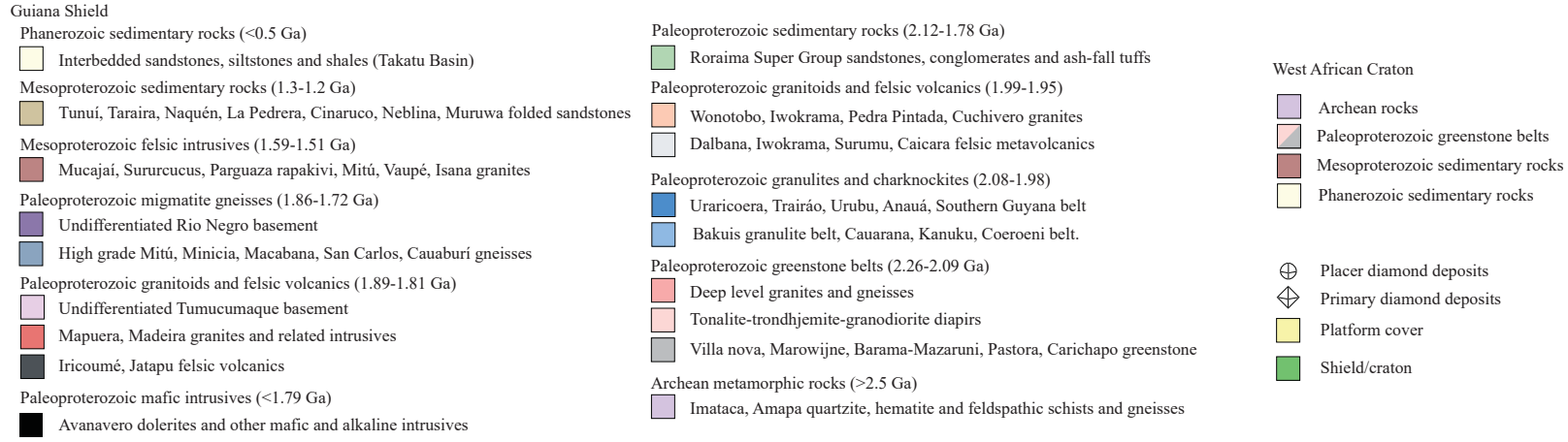

Figure 2

This is the peer-reviewed, final accepted version for American Mineralogist, published by the Mineralogical Society of America.
The published version is subject to change. Cite as Authors (Year) Title. American Mineralogist, in press.
DOI: https://doi.org/10.2138/am-2020-7486. http://www.minsocam.org/

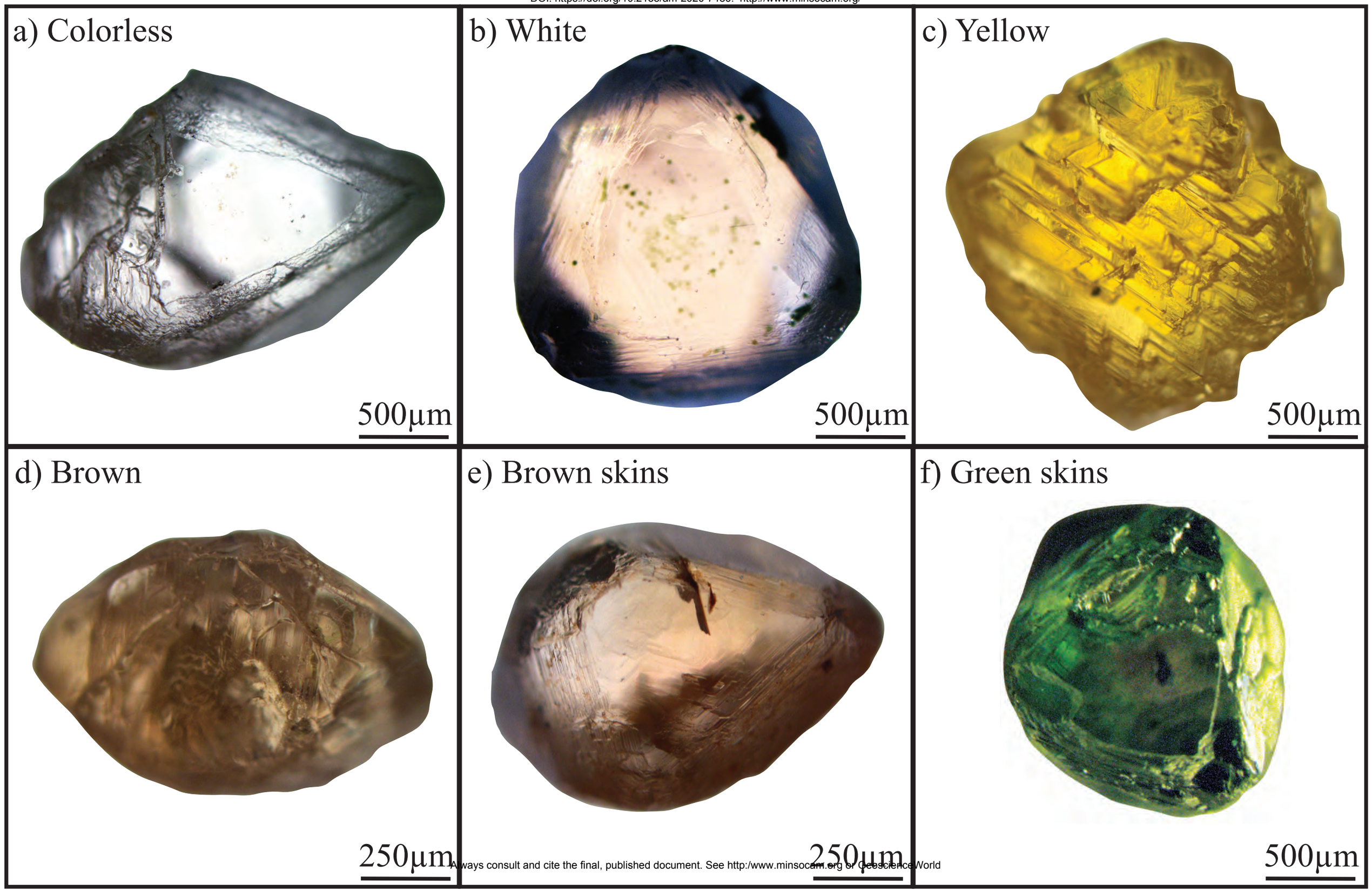

This is the peer-reviewed, final accepted version for American Mineralogist, published by the Mineralogical Society of America.
The published version is subject to change. Cite as Authors (Year) Title. American Mineralogist, in press.
DOI: https://doi.org/10.2138/am-2020-7486. http://www.minsocam.org/

Figure 3

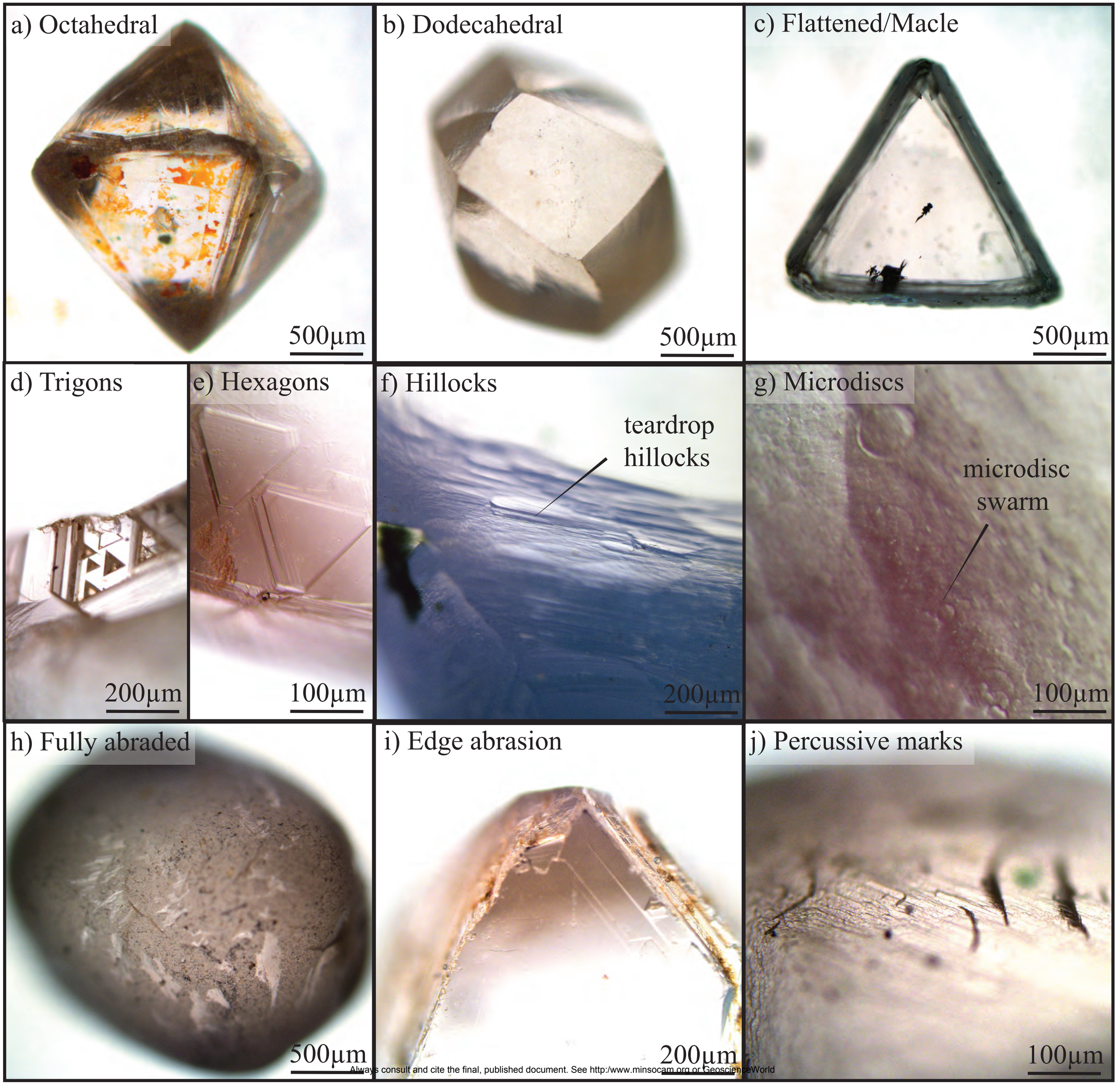

Figure 4

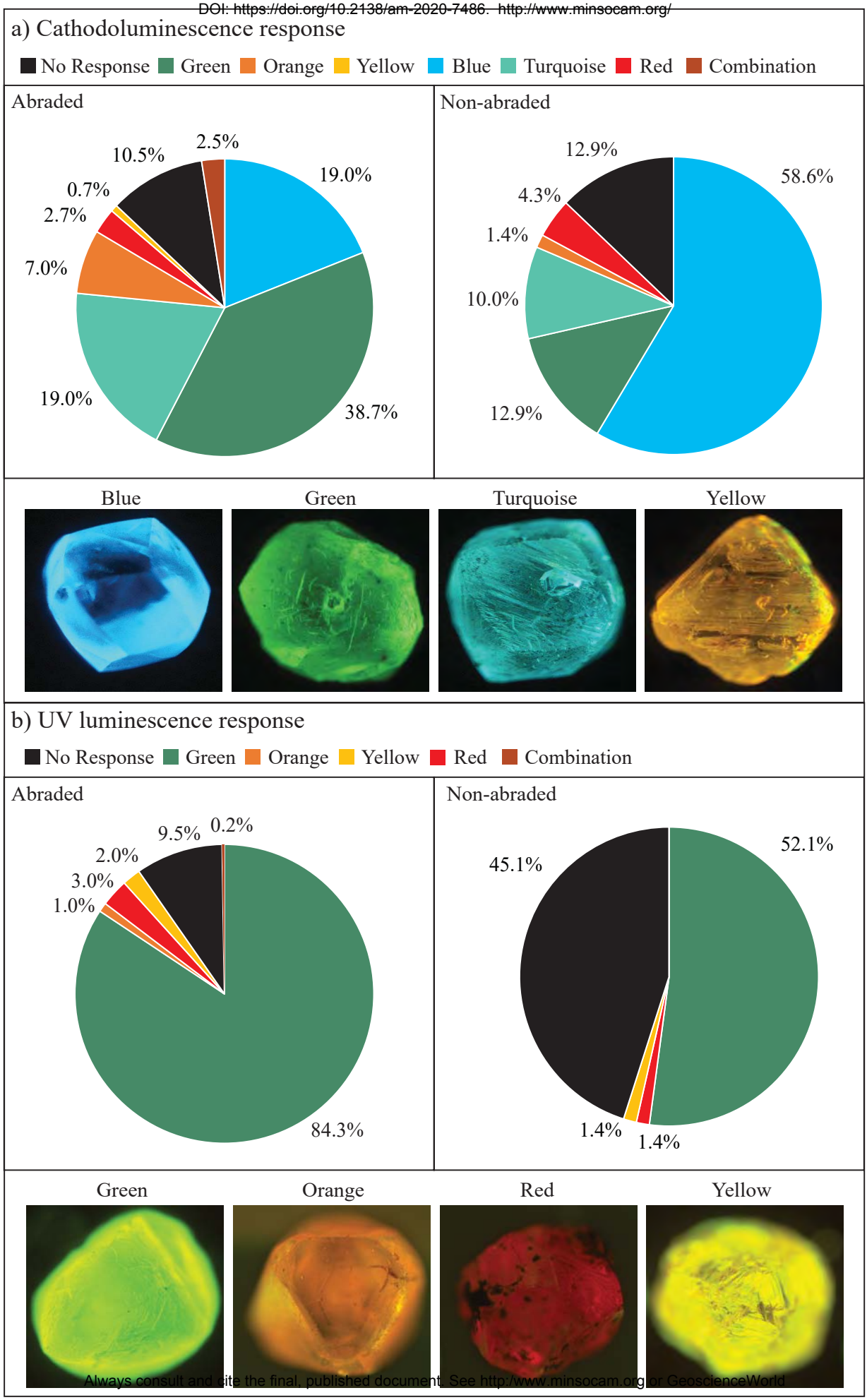

This is the peer-reviewed, final accepted version for American Mineralogist, published by the Mineralogical Society of America.
The published version is subject to change. Cite as Authors (Year) Title. American Mineralogist, in press.
DOI: https://doi.org/10.2138/am-2020-7486. http://www.minsocam.org/

Figure 5

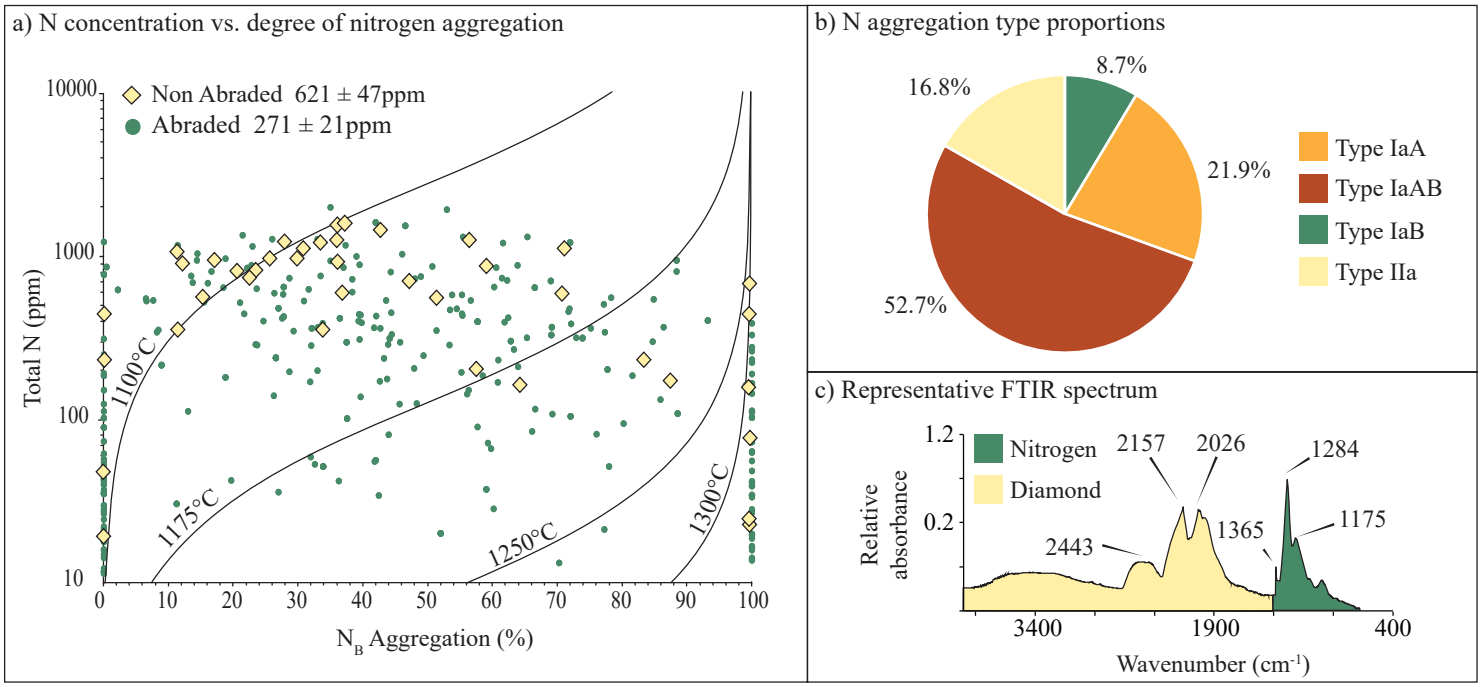

This is the peer-reviewed, final accepted version for American Mineralogist, published by the Mineralogical Society of America.
The published version is subject to change. Cite as Authors (Year) Title. American Mineralogist, in press.
DOI: https://doi.org/10.2138/am-2020-7486. http://www.minsocam.org/

Figure 6

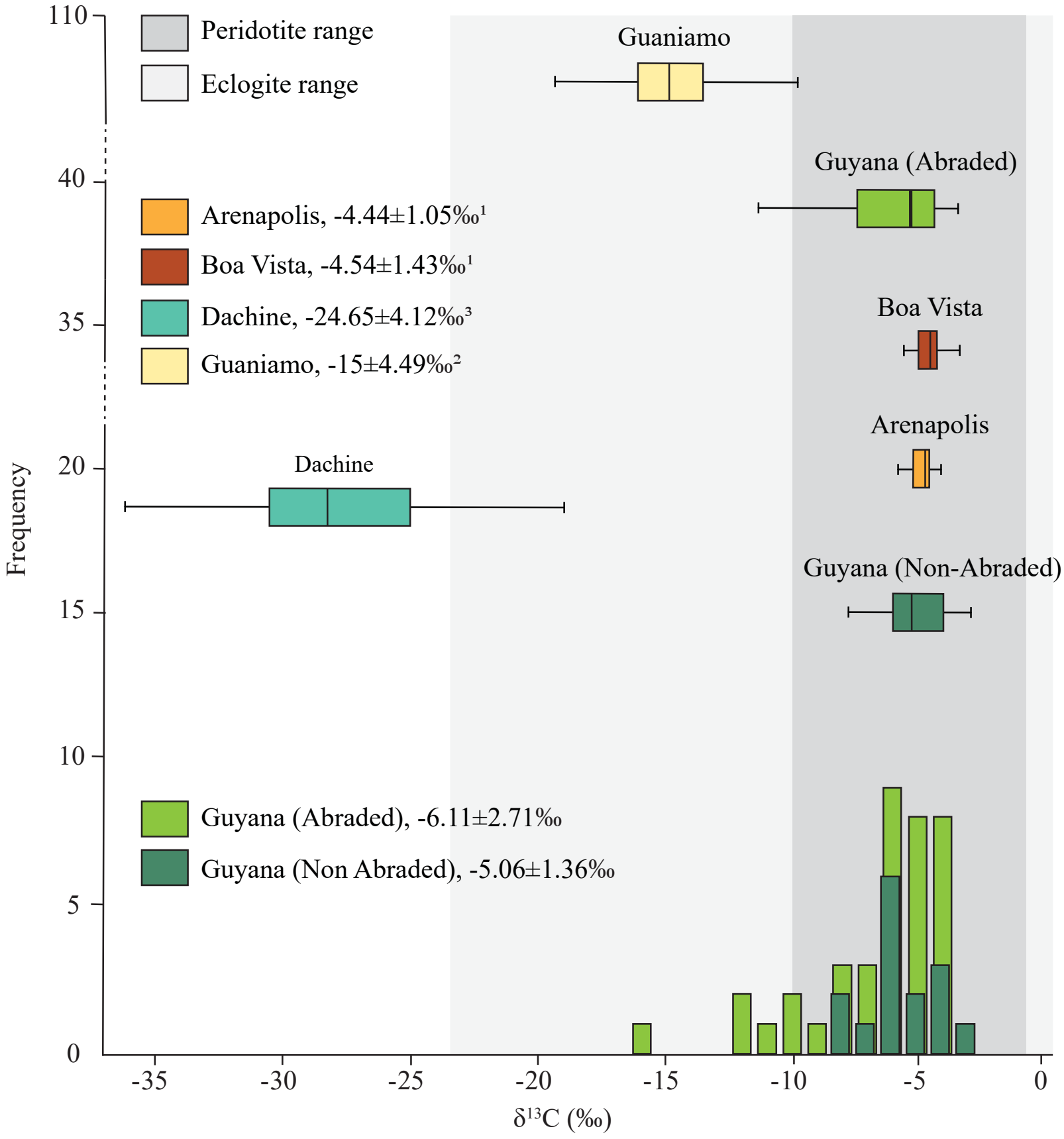

This is the peer-reviewed, final accepted version for American Mineralogist, published by the Mineralogical Society of America.
The published version is subject to change. Cite as Authors (Year) Title. American Mineralogist, in press.
DOI: https://doi.org/10.2138/am-2020-7486. http://www.minsocam.org/

Figure 7

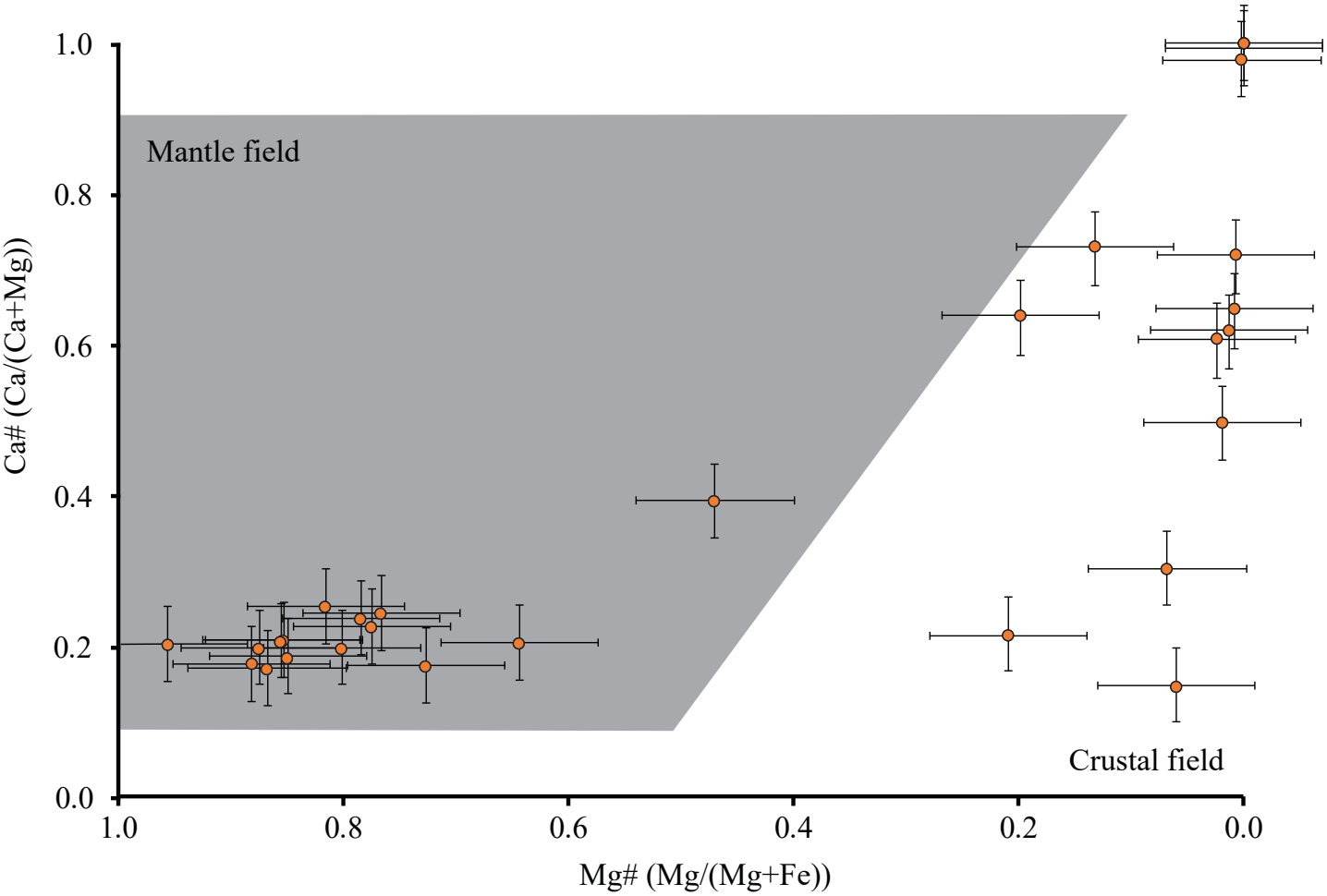

Figure 8

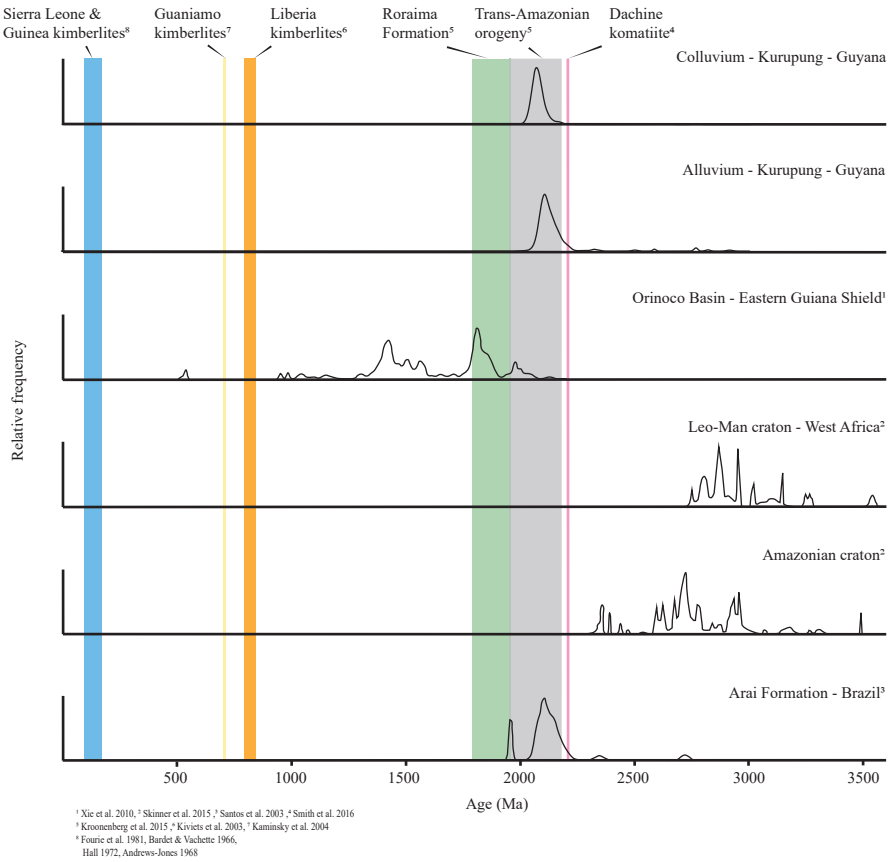

This is the peer-reviewed, final accepted version for American Mineralogist, published by the Mineralogical Society of America.
The published version is subject to change. Cite as Authors (Year) Title. American Mineralogist, in press.
DOI: https://doi.org/10.2138/am-2020-7486. http://www.minsocam.org/

Table 1. Summary morphology

		Color							Habit						Spotting				Late Stage Etching		Sedimentilogical abrasion	
Location	*n*	B	Br	Y	Gr	P	W	X	O	D	Co	C	Fl	Unk	Gr	Br	Co	X	Etching	No Etching	Abraded	Non Abraded
Ekereku	*226*	0	9	6	0	0	0	211	69	103	29	9	11	5	97	9	18	205	90	208	159	53
Jawalla	*19*	0	1	2	0	0	0	16	6	7	4	1	1	0	8	0	0	11	6	13	19	0
Kamarang	*154*	0	6	2	0	0	1	145	44	16	35	0	40	19	95	4	9	46	53	101	140	13
Konawaruk	*6*	0	0	0	0	0	0	6	3	1	0	0	2	0	3	0	1	2	0	5	6	0
Kurupung	*81*	0	1	4	0	0	1	75	25	17	11	3	18	8	30	2	6	90	28	55	78	5
Maikwak	*3*	0	0	0	0	0	1	2	1	2	0	0	0	0	3	0	0	0	0	3	3	0
Monkey Mt.	*3*	0	0	0	0	0	0	3	2	1	0	0	0	0	2	0	0	1	0	3	3	0
%		0.0	3.5	2.8	0.0	0.0	0.6	92.7	30.4	29.8	16.0	2.6	14.6	6.5	37.1	2.3	5.3	55.3	31.3	68.7	85.2	14.8

B - blue, Br - brown, Y - yellow, P - pink, W - White , X - no colour/spotting

O - octahedral, D - dodecahedral, Co - combination, C - cubic, Fl - flattened/elongate, Unk - unknown

This is the peer-reviewed, final accepted version for American Mineralogist, published by the Mineralogical Society of America.
The published version is subject to change. Cite as Authors (Year) Title. American Mineralogist, in press.
DOI: https://doi.org/10.2138/am-2020-7486. http://www.minsocam.org/

Table 2. Pit dissolution textures of Guyana's diamonds

Type	Trigons	Tetragons	Hexagons	Trapezoids
Point Bottom (%)				
very fine (< 25 μm)	7.7	1.3	0.0	0.0
fine (25 - 50 μm)	2.6	3.8	0.0	0.0
medium (50 - 75 μm)	1.3	5.1	1.3	0.0
coarse (75 - 100 μm)	0.0	6.4	0.0	0.0
very coarse (> 100 μm)	0.0	1.3	0.0	0.0
Total %	11.5	17.9	1.3	0.0
Flat Bottom (%)				
very fine (< 25 μm)	5.1	0.0	5.1	0.0
fine (25 - 50 μm)	14.1	0.0	9.0	5.1
medium (50 - 75 μm)	5.1	0.0	1.3	1.3
coarse (75 - 100 μm)	11.5	3.8	3.8	0.0
very coarse (> 100 μm)	1.3	0.0	1.3	1.3
Total %	37.2	3.8	20.5	7.7

error ±5 μm, # of diamonds - 370, # of diamonds with dissolution pits - 78

This is the peer-reviewed, final accepted version for American Mineralogist, published by the Mineralogical Society of America.
The published version is subject to change. Cite as Authors (Year) Title. American Mineralogist, in press.
DOI: https://doi.org/10.2138/am-2020-7486. http://www.minsocam.org/

Table 3. Optical spectroscopy

	Cathodoluminescence								UV flourescence						*n*
Location	B	Gr	T	O	R	Y	X	Z	Gr	O	R	Y	X	Z	
Ekereku	80	53	32	9	3	1	28	2	154	1	3	1	50	0	*209*
Jawalla	3	4	7	4	0	0	0	1	18	1	0	0	0	0	*19*
Kamarang	20	66	26	12	5	1	19	3	127	0	7	5	13	1	*152*
Konawaruk	1	3	1	0	0	0	1	0	6	0	0	0	0	0	*6*
Kurupung	10	36	16	4	6	1	3	4	65	2	3	3	7	0	*80*
Maikwak	1	2	0	0	0	0	0	0	3	0	0	0	0	0	*3*
Monkey Mt.	2	0	1	0	0	0	0	0	3	0	0	0	0	0	*3*
%	24.8	34.8	17.6	6.2	3.0	0.6	10.8	2.1	79.5	0.8	2.7	1.9	14.8	0.2	

Cathodoluminescence, n - 471, UV flourescence, n - 473

B - blue, Gr - green, T - turquoise, Y - yellow, O - orange, R - red , X - no response, Z - combination

Table 4. Spectroscopic comparisons between abraded and non-abraded diamonds

Spectroscopy	**Abraded**		**Non-abraded**	
FTIR[1]	**N (ppm)**	***n***	**N (ppm)**	***n***
mean	271 ± 21	*349*	621 ± 47	*44*
median	109		590	
σ	353		473	
skewness	1.82		0.26	
kurtosis	6.62		1.91	
FMM populations				
Pop. 1	1911 ± 150	*2*	—	—
Pop. 2	1234 ± 99	*16*	—	—
Pop. 3	—	—	968 ± 79	*18*
Pop. 4	610 ± 52	*54*	604 ± 48	*7*
Pop. 5	351 ± 29	*60*	390 ± 26	*4*
Pop. 6	193 ± 16	*30*	180 ± 16	*6*
Pop. 7	84 ± 8	*34*	—	—
Pop. 8	39 ± 3	*46*	47 ± 3	*1*
Pop. 9	21 ± 2	*26*	23 ± 1	*4*
Pop. 10	13 ± 1	*16*	—	—
Pop. 11	6 ± 0.4	*5*	4 ± 0.3	*2*
Cathodoluminescence[2]	**%**	***n***	**%**	***n***
Blue	19.0	*76*	58.6	*41*
Green	38.7	*155*	12.9	*9*
Turquoise	19.0	*76*	10.0	*7*
Orange	7.0	*28*	1.4	*1*
Red	2.7	*11*	4.3	*3*
Yellow	0.7	*3*	—	—
No Response	10.5	*42*	12.9	*9*
Combination	2.5	*10*	—	—
UV luminescence	**%**	***n***	**%**	***n***
Blue	—	—	—	—
Green	84.3	*339*	52.1	*37*
Turquoise	—	—	—	—
Orange	1.0	*4*	—	—
Red	3.0	*12*	1.4	*1*
Yellow	2.0	*8*	1.4	*1*
No Response	9.5	*38*	45.1	*32*
Combination	0.2	*1*	—	—

[1] Abraded vs Non-abraded log N (ppm), |t|-test statistic: 12.7 > |t|-threshold value: 1.3, with 95% compatibility interval and $p < .00001$

[2] Abraded vs Non-abraded CL (%), $\chi 2$- test statistic: 287 > $\chi 2$-threshold value: 14.1, with 7 degrees of freedom, a 90% compatibility interval, and $p < .00001$

Table 5. Guyana diamond inclusion types

Inclusion	# of diamonds	Paragenesis
Chromite	*11*	Peridotitic
Enstatite[1]	*15*	Peridotitic
Forsterite[2]	*42*	Peridotitic
Cr-pyrope garnet	*3*	Peridotitic
Almandine garnet	*1*	Eclogitic
Coesite	*1*	Eclogitic
Clinopyroxene	*1*	Eclogitic
Rutile	*15*	Eclogitic

[1]Raman spectra doublet peaks indicate a more Mg rich and enstatite composition. [2]Raman spectra doublet peak and lower intensity of ν3 mode peak suggest a more forsteritic composition (Mg# ~ 90)

This is the peer-reviewed, final accepted version for American Mineralogist, published by the Mineralogical Society of America.
The published version is subject to change. Cite as Authors (Year) Title. American Mineralogist, in press.
DOI: https://doi.org/10.2138/am-2020-7486. http://www.minsocam.org/

Table 6. Nitrogen concentrations of Guiana Shield diamonds

Location	Total N ± σ (ppm)	$\%N_B$	n
Guyana			
Ekereku	407 ± 472	38 ± 34	*134*
Jawalla	123 ± 201	27 ± 34	*19*
Kamarang	275 ± 310	38 ± 34	*150*
Kurupung	242 ± 352	36 ± 41	*79*
Konawaruk	249 ± 265	18 ± 19	*6*
Maikwak	250 ± 78	34 ± 5	*3*
Monkey Mt.	610 ± 138	65 ± 16	*3*
Venezuela			
Los Coquitos[1]	641 ± 324	62 ± 19	*77*
Guaniamo[2]	620	69	*192*
French Guiana			
Dachine[3]	20 ± 29	NA	*18*
Brazil			
Boa Vista[4]	345 ± 412	39 ± 30	*34*

[1] Kaminsky et al 2006, [2] Kaminsky et al 2000, [3] Smith et al 2016, [4]Kaminsky et al 2001, [4]Tappert et al 2006

This is the peer-reviewed, final accepted version for American Mineralogist, published by the Mineralogical Society of America.
The published version is subject to change. Cite as Authors (Year) Title. American Mineralogist, in press.
DOI: https://doi.org/10.2138/am-2020-7486. http://www.minsocam.org/

Table 7. Formation temperatures of Guiana Shield diamonds

Location	T (ºC)	n	Derivation
Guyana			
Abraded	1128 ± 104	*208*	N aggregation (1.3Ga residence)
Non-abraded	1101 ± 72	*34*	N aggregation (2.6Ga residence)
mean	1124 ± 100	*242*	
median	1148	*242*	
skewness	-1.49	*242*	
kurtosis	1.72	*242*	
Brazil[1]			
Boa Vista	1208 ± 74	*27*	Chromite-Olivine inclusion equilibration
Venezuela[2]			
Guaniamo	1116 ± 99	*6*	Garnet-Diopside inclusion equilibration

[1] Tappert et al 2006, [2] Kaminsky et al 2000